Monthly Notices of the ROYAL ASTRONOMICAL SOCIETY

Mon. Not. R. Astron. Soc. **413,** 3075–3094 (2011) doi:10.1111/j.1365-2966.2011.18381.x

Effects of the explosion asymmetry and viewing angle on the Type Ia supernova colour and luminosity calibration★

Keiichi Maeda,[1]† Giorgos Leloudas,[2] Stefan Taubenberger,[3] Maximilian Stritzinger,[2,4,5] Jesper Sollerman,[2,4] Nancy Elias-Rosa,[6] Stefano Benetti,[7] Mario Hamuy,[8] Gaston Folatelli[1,8] and Paolo A. Mazzali[3,9]

[1]*Institute for the Physics and Mathematics of the Universe (IPMU), Todai Institutes for Advanced Study (TODIAS), University of Tokyo, 5-1-5 Kashiwanoha, Kashiwa, Chiba 277-8583, Japan*
[2]*Dark Cosmology Centre, Niels Bohr Institute, Copenhagen University, Juliane Maries Vej 30, 2100 Copenhagen Ø, Denmark*
[3]*Max-Planck-Institut für Astrophysik, Karl-Schwarzschild-Straße 1, 85741 Garching, Germany*
[4]*The Oskar Klein Centre, Department of Astronomy, Stockholm University, AlbaNova, 10691 Stockholm, Sweden*
[5]*Carnegie Observatories, Las Campanas Observatory, Casilla 601, La Serena, Chile*
[6]*Institut de Ciències de l'Espai (IEEC-CSIC), Campus VAB, 08193 Bellaterra, Spain*
[7]*INAF - Osservatorio Astronomico di Padova, vicolo dell'Osservatorio 5, I-35122 Padova, Italy*
[8]*Departamento de Astronomía, Universidad de Chile, Casilla 36-D, Santiago, Chile*
[9]*Scuola Normale Superiore, Piazza Cavalieri 7, 56127 Pisa, Italy*

Accepted 2011 January 18. Received 2011 January 18; in original form 2010 February 12

ABSTRACT

Phenomenological relations exist between the peak luminosity and other observables of type Ia supernovae (SNe Ia) that allow one to standardize their peak luminosities. However, several issues are yet to be clarified: SNe Ia show colour variations after the standardization. Also, individual SNe Ia can show residuals in their standardized peak absolute magnitude at the level of $\sim$0.15 mag. In this paper, we explore how the colour and luminosity residual are related to the wavelength shift of nebular emission lines observed at $\gtrsim$150 d after the maximum light. A sample of 11 SNe Ia which likely suffer from little host extinction indicates a correlation (3.3σ) between the peak $B-V$ colour and the late-time emission-line shift. Furthermore, a nearly identical relation applies for a larger sample in which only three SNe with $B-V \gtrsim 0.2$ mag are excluded. Following the interpretation that the late-time emission-line shift is a tracer of the viewing direction from which an off-centre explosion is observed, we suggest that the viewing direction is a dominant factor controlling the SN colour and that a large part of the colour variations is intrinsic, rather than due to the host extinction. We also investigate a relation between the peak luminosity residuals and the wavelength shift in nebular emission lines in a sample of 20 SNe. We thereby found a hint of a correlation (at $\sim 1.6\sigma$ level). The confirmation of this will require a future sample of SNe with more accurate distance estimates. Radiation transfer simulations for a toy explosion model where different viewing angles cause the late-time emission-line shift are presented, predicting a strong correlation between the colour and shift, and a weaker one for the luminosity residual.

Key words: supernovae: general – cosmological parameters – distance scale.

1 INTRODUCTION

Type Ia supernovae (SNe Ia) are used to measure cosmological parameters and study the nature of the dark energy (see Leibundgut 2008, and references therein). Thanks to the uniformity of their peak luminosities, once a phenomenological relation between the light-curve shape and the peak luminosity is applied (hereinafter the light-curve correction or the Phillips relation), they can be accurately used as cosmological standard candles (Phillips 1993; Hamuy et al. 1996; Phillips et al. 1999). Their colours are also known to correlate with the light-curve shape (Tripp 1998; Phillips et al. 1999; Tripp & Branch 1999). In addition to the light-curve shape and colour, several other observables, mostly related to spectral features, have been shown to correlate with the SN peak luminosity (e.g. Nugent

★Partially based on observations obtained at the Gemini Observatory, Cerro Pachon, Chile (Gemini Programs GS-2008B-Q-8, GS-2008B-Q-32, GS-2008B-Q-56 and GS-2009B-Q-40).
†E-mail: keiichi.maeda@ipmu.jp

et al. 1995; Mazzali et al. 1998; Benetti et al. 2005; Bongard et al. 2006; Hachinger, Mazzali & Benetti 2006; Foley, Filippenko & Jha 2008).

Currently, there are several issues yet to be clarified. One central issue is that the intrinsic colour variations of SNe Ia have not yet been fully understood. After the application of the relation between colour and light curve shape, there remain variations in the colour excess of SNe Ia. So far, it has been practically impossible to discriminate between the contributions from a possible 'residual' intrinsic colour, which does not correlate with the light-curve shape, and that from the extinction within the host or the environment around the SN. This issue could be related to the fact that when the dispersion of the Hubble diagram is minimized with R_V being treated as a free parameter, one obtains low values of R_V between 1–2. However, as shown by Folatelli et al. (2010; hereainfter F10), when one compares the colours or colour excesses of normal SNe Ia, a more typical Milky Way like value of the reddening law is obtained, that is, $R_V \sim 3$. F10 argued that this apparent discrepancy suggests that there is an intrinsic colour variation within SNe Ia that correlates with the luminosity, but is independent of the light-curve decline rate Δm_{15} (B).[1] In this study, we adopt an $R_V = 1.72$ as derived from F10 (i.e. Calibration 7 of Table 9).

Moreover, after the application of the light-curve correction, Hubble diagram residuals at the level of ∼0.15 mag exist for individual SNe Ia (e.g. Phillips et al. 1999; Prieto, Rest & Suntzeff 2006; Jha, Riess & Kirshner 2007; Hicken et al. 2009a,b). This is one of the issues that presently limit the precision in using SNe Ia to constrain the value of the equation-of-state parameter of the dark energy (e.g. Hicken et al. 2009b; see also Wood-Vasey et al. 2007; Kessler et al. 2009, for the current status of the precision in SN Ia cosmology). Several suggestions have been made for a secondary parameter that may provide a more accurate luminosity calibration[2] (or on parameters already including the effect of the second parameter). Suggestions include (i) metallicity (Timmes, Brown & Truran 2003; Gallagher et al. 2005; Mazzali & Podsiadlowski 2006; Höflich et al. 2010, but see also Howell et al. 2009; Neill et al. 2009; Yasuda & Fukugita 2010); (ii) high-velocity spectral features (Wang et al. 2009b); (iii) spectral flux ratios (Bailey et al. 2009; Yu, Yang & Lu 2009); and (iv) the mass and/or the morphological type of the host galaxy (Kelly et al. 2010; Lampeitl et al. 2010; Sullivan et al. 2010).

An interesting possibility for the origin of the diverse properties of SNe Ia was recently suggested by Kasen, Röpke & Woosley (2009) theoretically and by Maeda et al. (2010a,b, hereinafter M10a and M10b, respectively) observationally, namely an asymmetry in the SN explosion combined with the observer viewing angle. In particular, M10a identified potential signatures of asymmetry in a number of SNe Ia, based on the observed wavelength shift of late-time emission lines (see Section 2 for more details). M10a and M10b showed that the required configuration is qualitatively consistent with the expectation from a deflagration-to-detonation transition scenario[3] if the first thermonuclear sparks are ignited offset from the centre of the progenitor white dwarf.

M10b suggested that the viewing angle effect is a probable origin of the spectral evolution diversity of SNe Ia. Different SNe Ia show different velocity gradients ($\dot{v}_{\rm Si}$), defined as the speed of the decrease in the Si II absorption velocity after the maximum brightness (Benetti et al. 2005; see also Branch, Drucker & Jeffery 1988). SNe are divided into high-velocity-gradient (HVG) ($\dot{v}_{\rm Si} > 70\,{\rm km\,s^{-1}\,day^{-1}}$) and low-velocity-gradient (LVG) objects ($\dot{v}_{\rm Si} < 70\,{\rm km\,s^{-1}\,day^{-1}}$). M10b argued that different velocity gradients are a consequence of different viewing directions from which the SN is observed. It has been indicated that LVG and HVG SNe may show different properties in their intrinsic colours (e.g. Pignata et al. 2008) and that their luminosities may have to be calibrated in a different manner (Wang et al. 2009b). Here we revisit this colour issue in the context of our new interpretation of LVG and HVG SNe.

In this paper, we explore whether the late-time emission-line shift, and thereby the observer viewing angle on an asymmetric explosion, is related to the intrinsic colour and the luminosity residuals of SNe Ia after the application of the Phillips relation. We find a correlation between the colour at the maximum brightness and the nebular emission-line shift. We also investigate a possible relation between the luminosity residuals and the nebular line shifts, but since our sample is small, the significance is not overwhelming. We then investigate the ramification of the viewing angle on the luminosity and colour calibrations with the help of multidimensional radiation transfer calculations and find that the predicted effect is qualitatively consistent with the trends seen in the data.

This paper is organized as follows. In Section 2, we summarize the findings of M10a regarding the asymmetry in SNe Ia, which are then used throughout this paper. In Section 3, we present details of the sample of nearby SNe Ia considered in this study. In Section 4, we discuss how the viewing angle is related to the intrinsic colour of SNe Ia. In Section 5, we discuss the procedures to estimate the intrinsic absolute magnitude and subsequent residuals. In Section 6, we compare the late-time emission-line shifts with the luminosity residuals. In Section 7, we investigate the effect of the viewing angle on the peak brightness and colour by simulating light curves for kinematic off-centre toy models. In Section 8, this paper is closed with conclusions, discussion and future perspectives.

2 ASYMMETRY IN TYPE Ia SNE

In this section, we summarize the findings presented in M10a regarding the asymmetry in SNe Ia. M10a suggested that the innermost region of the ejecta, filled with stable Fe-peak elements, is generally offset and that an observer's viewing angle can be traced by shifts in the central wavelengths of nebular emission lines of [Fe II] λ7155 and [Ni II] λ7378 at late phases. The argument is as follows:

(i) Using a sample of late-time (i.e. at least 100 d after the maximum brightness) SN Ia spectra, mostly drawn from the Online Supernova Spectrum Archive (SUSPECT) data base,[4] M10a found that in cases where the [Fe II] λ7155 and [Ni II] λ7378 lines were

[1] $\Delta m_{15}(B)$ is the magnitude difference in the B band between the maximum brightness and 15 d later.

[2] Indeed, this is the 'third' parameter, since light-curve fitting methods usually use two parameters: the light-curve shape and colour. In this paper, we simply call the additional parameter the 'second' parameter following the convention.

[3] In the deflagration-to-detonation transition scenario, the thermonuclear sparks first trigger the deflagration flames which travel subsonically and then the flames subsequently turn into a supersonic detonation flame (Khokhlov 1991).

[4] The SUSPECT data base is found at http://bruford.nhn.ou.edu/∼suspect/.

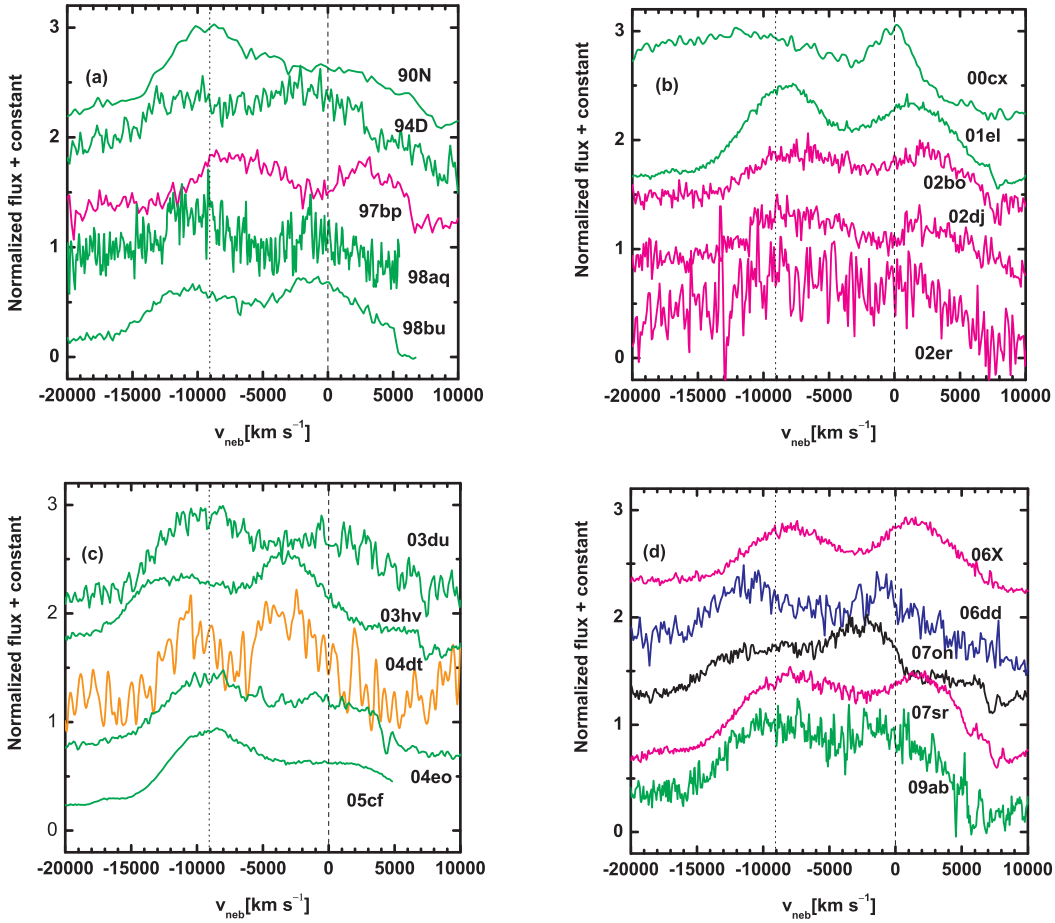

Figure 1. [Fe II] λ7155 and [Ni II] λ7378 in late-time spectra of SNe Ia (see references in Table 1). The spectra have been redshift-corrected and then converted into a velocity assuming 7378 Å as the zero-velocity. The rest positions of [Fe II] and [Ni II] are denoted by the dotted and dashed lines, respectively. The colour coding indicates the early-phase 'velocity gradient' (see Section 1; Benetti et al. 2005): LVG SNe in green and HVG SNe in magenta. SN 2007on is a fast-declining SN 1986G-like SN Ia (Morrell, Folatelli & Stritzinger 2007) and is shown in black. SN 2006dd, without a measured velocity gradient, is shown in blue. SN 2004dt, which was argued to be a peculiar outlier based on late-time spectra (M10b), is shown in orange.

detected, they exhibited measurable shifts in their central wavelength with respect to the expected rest wavelength, as shown in Fig. 1. There is no clear correlation between the phase of the nebular spectrum and the shift of the [Fe II] λ7155 and [Ni II] λ7378 lines. In addition, no significant evolution is seen in the measured line shifts for individual SNe Ia at $\gtrsim$150 d. To illustrate these characteristics, we show the wavelength shifts (converted to a velocity) of these lines in Fig. 2.

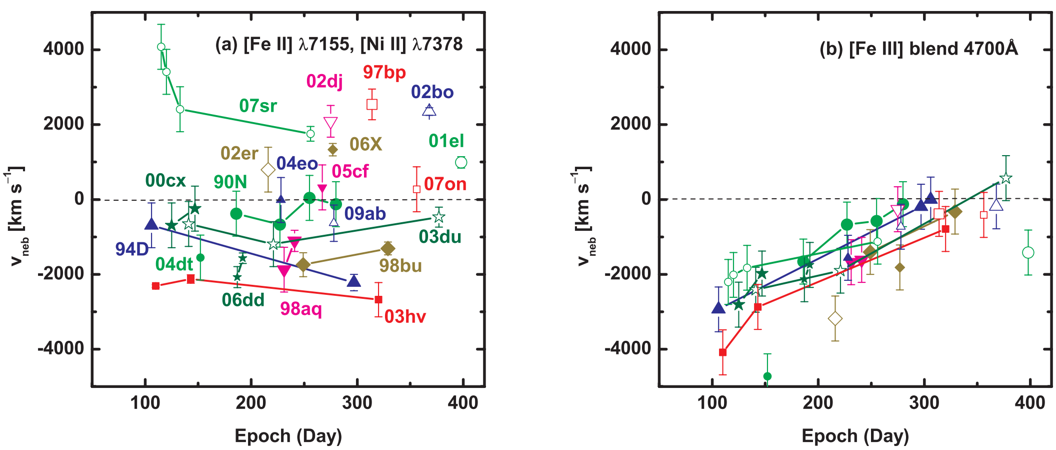

Figure 2. Observed wavelength shifts for (a) the [Fe II] λ7155 and [Ni II] λ7378 lines and (b) the [Fe III] blend at 4700 Å, plotted as a function of time since the *B*-band maximum. The wavelengths have been converted to velocities, assuming the expected rest wavelengths of the lines as the zero-velocity. The same objects are connected by lines. The data are from our present sample (see Section 3, Table 1 and references therein).

(ii) On the other hand, the strongest lines at late phases, that is, the [Fe III] blend at ∼4700 Å and the [Fe II]/[Fe III] blend at ∼5250 Å, behave similarly for all SNe Ia. Since the [Fe III] blend at ∼4700 Å is stronger and its blended nature can be better handled (M10a), we show its temporal evolution in Fig. 2. There is a clear correlation between the phase of the nebular spectrum and the central wavelength of the [Fe III] blend at 4700 Å, unlike for [Fe II] λ7155 and [Ni II] λ7378. The shifts of [Fe III] at 4700 Å evolve from the blue to the rest wavelength for all SNe.

(iii) The temporal behaviour seen in Fig. 2 suggests that the shifts of [Fe II] λ7155 and [Ni II] λ7378 trace the line-of-sight velocity of the emitting material. As a consequence, the diversity in the wavelength shifts indicates that the distribution of the emitting material is offset with respect to the centre of the SN ejecta. Note that spherically symmetric explosions with different expansion velocities should produce different line widths, but never a shift in the central wavelength. As a result of the offset, the observed diversity arises from different observer viewing angles. On the contrary, the observed features of the [Fe III] blend at 4700 Å suggest that the [Fe III] blend traces the distribution of the emitting material only at sufficiently late epochs and the small diversity indicates that the emitting material is distributed more or less spherically.

M10a argued that these characteristics can be naturally explained by a deflagration-to-detonation explosion scenario, if the distribution of the inner deflagration ash has an offset and the outer detonation ash is distributed in a roughly spherically symmetric way. They proposed that these lines are emitted from different regions – an outer, relatively low density region dominated by radioactive ^{56}Ni (which decays into ^{56}Co and then into ^{56}Fe, powering the SN light curve) and an inner, relatively high density region dominated by stable Fe-peak elements, that is, ^{58}Ni, ^{56}Fe and ^{54}Fe (see also Mazzali et al. 2007). The former and latter correspond to the detonation and the deflagration ashes, respectively. For such a configuration, the outer region should be in a relatively high ionization state (i.e. doubly ionized) and at high temperature (electron temperature $T_{\rm e} \gtrsim 10\,000$ K). On the other hand, the inner region should be in a low ionization state (i.e. singly ionized) and at low temperature ($T_{\rm e} \sim 2000$–7000 K). This stems from (a) the ionization balance; and (b) the thermal balance, namely (a) $n_{i+1}/n_i \propto J_\gamma n_{\rm e}^{-1}$, where n_i is the density of the ith ionization state, J_γ is the radioactive energy input from the decay chain $^{56}{\rm Ni} \rightarrow {}^{56}{\rm Co} \rightarrow {}^{56}{\rm Fe}$ and $n_{\rm e}$ is the electron density; and (b) ${\rm e}^{-T_{\rm ex}/T_{\rm e}} \propto J_\gamma n_{\rm e}^{-1} n_0^{-1}$, where $T_{\rm ex}$ is the excitation temperature of the line and n_0 is the population of the lower level.

The [Fe III] blend at 4700 Å is emitted by $\rm Fe^{++}$ with high $T_{\rm ex}$ and thus the outer region dominates the emission of this blend. This blend is thus attributed to the emission from the detonation ash in the deflagration-to-detonation transition scenario. The opposite is true for [Fe II] λ7155 and [Ni II] λ7378, and thus these lines are mostly emitted from the inner region, that is, the deflagration ash. Combined with the phenomenologically derived distribution of the material emitting these lines (see above), this argues that the deflagration ash is located offset from the centre of the progenitor star, while the detonation ash is distributed spherically.

Although these arguments are based on a few lines in the optical wavelength regime, this interpretation predicts that, at late phases, the lines from high ionization states and/or with high excitation temperature should show virtually no shift, while those from low ionization states and/or with low excitation temperature show a wavelength shift depending on the viewing direction. M10a showed that this is the case for SN 2003hv, which has a well-observed spectrum at late phases, covering spectral lines from the optical all the way to the mid-infrared (MIR) (Motohara et al. 2006; Gerardy et al. 2007; Leloudas et al. 2009). The size of the offset derived for SN 2003hv was found to be ∼3500 km s^{-1} (M10a). Note that this behaviour in various lines from the optical through MIR provides an additional argument against line blending and radiation transfer as a cause of the observed line shifts.

This finding was interpreted as evidence that the initial deflagration flame proceeds in an asymmetric way, having an offset with respect to the explosion centre, in the context of a deflagration-to-detonation transition explosion scenario (Khokhlov 1991; Yamaoka et al. 1992; Woosley & Weaver 1994; Iwamoto et al. 1999; Röpke & Niemeyer 2007; Kasen et al. 2009; Seitenzahl et al. 2010). Although the details of the ignition process are not yet fully understood, theoretically, an off-centre ignition may be a natural consequence of the convection within a progenitor white dwarf (Kuhlen, Woosley & Glatzmaier 2006). Maeda et al. (2010c) (hereinafter M10c) argued, based on their hydrodynamic and nucleosynthesis simulations, that a deflagration-to-detonation transition model with the initial sparks ignited at an offset from centre will result in a configuration qualitatively consistent with the above findings.

According to this interpretation and an extensive search of emission lines from the optical to MIR wavelengths, M10a suggested that the best lines to use in the optical for probing the asymmetry in the innermost SN ejecta are [Fe II] λ7155 and [Ni II] λ7378 (as well as [Fe II] λ8621; Leloudas et al. 2009). These are the only ones which satisfy the criteria that (a) they reflect the low ionization and low temperature; (b) they suffer from little blending; and (c) they are covered by most optical spectra. We therefore adopt these lines as diagnostics of the ejecta asymmetry and the viewing angle in this study.

3 SUPERNOVA SAMPLE

In this paper, we investigate how an asymmetric explosion and different viewing angles influence the colour and luminosity of SNe Ia, by examining correlations between these quantities and the emission-line shift in the late-time spectra. The sample of SNe Ia is thus limited by the requirement that late-time nebular spectra are available. Our initial late-time spectral data set comprised the same 20 SNe Ia used by M10a, mostly drawn from the SUSPECT data base, supplemented by other late-time nebular spectra accessible to the authors. To include these spectra in the present analysis, we imposed some additional criteria: (i) the spectrum was taken at $\gtrsim$150 d after the maximum brightness (see Fig. 2); (ii) either [Fe II] λ7155 or [Ni II] λ7378 could be identified; (iii) the spectra had to be of high enough quality that the central wavelength of either of these lines could be measured; (iv) the SNe were required to have good early-phase B- and V-band photometry so that their light-curve parameters and colour at maximum could be estimated; and (v) $\Delta m_{15}(B)$ was in the range 0.7–1.7 mag in order to apply the well-developed relations between $\Delta m_{15}(B)$ and the peak absolute magnitude/colour (e.g. Phillips et al. 1999; F10).

From the initial data set, 13 objects fulfilled these criteria. In addition, we included seven SNe which satisfied our criteria, that is, SNe 1997bp, 2002bo, 2006X, 2006dd, 2007on, 2007sr and 2009ab. In 13 out of these 20 objects, both [Ni II] λ7378 and [Fe II] λ7155 were securely identified (see below). In the other seven events, only one of these lines was discernable. These seven SNe Ia were included in our analysis because a measurement of their nebular line velocity shift was possible, although less secure than when both lines were identified. The sample of 20 SNe Ia used in this

Table 1. SN Ia sample.

SN	Host	z	μ^a (mag)	$\Delta m_{15}(B)^b$ (mag)	V^c (mag)	$B-V^c$ (mag)	Reference[d]	$v_{\rm neb}$ (km s^{-1})	Reference[e]
1990N	NGC 4639	0.003 395	31.71 ± 0.15 (KP)	1.07 ± 0.05	12.62	0.037	L98	−126 ± 600	G96
1994D	NGC 4526	0.001 494	30.98 ± 0.20 (SBF)	1.32 ± 0.05	11.83	−0.080	R95, P96	−2220 ± 220	G96
1997bp	NGC 4680	0.008 312	32.68 ± 0.27 (HF)	0.97 ± 0.2	13.78	0.16	R05	2539 ± 410	M10b
1998aq	NGC 3982	0.003 699	31.56 ± 0.08 (KP)	1.12 ± 0.05	12.42	−0.11	R99	−1106 ± 286	B03
1998bu	NGC 3368	0.002 992	30.11 ± 0.20 (KP)	1.06 ± 0.05	11.80	0.34	J99, H00	−1309 ± 171	C01
2000cx	NGC 524	0.007 935	32.63 ± 0.27 (HF)	0.93 ± 0.04	12.99	0.10	L01	−244 ± 600	C03, S04
2001el	NGC 1448	0.003 896	31.23 ± 0.45 (TF)	1.13 ± 0.04	12.69	0.068	K03	993 ± 152	M05
2002bo	NGC 3190	0.004 240	31.70 ± 0.24 (SBF)[f]	1.16 ± 0.03	13.50	0.44	B04	2350 ± 100	S05
2002dj	NGC 5018	0.009 393	32.82 ± 0.25 (HF)	1.08 ± 0.05	13.85	0.063	P08	2090 ± 423	P08
2002er	UGC 10743	0.008 569	32.87 ± 0.25 (HF)	1.32 ± 0.03	14.10	0.16	P04	797 ± 600	K05
2003du	UGC 9391	0.006 384	32.42 ± 0.30 (HF)	1.02 ± 0.05	13.54	−0.089	A05, S07	−471 ± 265	S07
2003hv	NGC 1201	0.005 624	31.37 ± 0.30 (SBF)	1.61 ± 0.02	12.49	−0.035	L09	−2677 ± 457	L09
2004dt	NGC 799	0.019 730	34.55 ± 0.12 (HF)	1.21 ± 0.05	15.25	−0.053	A07	−1551 ± 600	A07
2004eo	NGC 6928	0.015 701	34.12 ± 0.14 (HF)	1.45 ± 0.04	15.02	0.064	P07a	−14 ± 600	P07a
2005cf	MCG-1-39-3	0.006 461	32.19 ± 0.33 (HF)	1.07 ± 0.03	13.26	−0.017	P07b, W09	324 ± 600	L07
2006X	NGC 4321	0.005 240	30.91 ± 0.20 (KP)	1.31 ± 0.05	13.96	1.34	W08, Y09	1331 ± 164	W08
2006dd	NGC 1316	0.005 871	31.26 ± 0.10 (PNLF)	1.08 ± 0.03	12.32	−0.060	S10a	−1569 ± 142	S10a
2007on	NGC 1404	0.006 494	31.45 ± 0.19 (SBF)	1.55 ± 0.01	12.98	0.12	S10b	272 ± 600	S10b
2007sr	NGC 4038	0.005 477	31.51 ± 0.17 (TRGB)	1.12 ± 0.01	12.54	0.12	S10b	1754 ± 198	S10b
2009ab	UGC 2998	0.011 171	33.29 ± 0.20 (HF)	1.25 ± 0.02	14.60	0.058	S10b	−634 ± 486	S10b

[a]Distance modulus from KP Cepheid measurements (KP), surface brightness fluctuations (SBF), the near-IR (NIR) Tully–Fisher relation (TF), the planetary nebulae luminosity function (PNLF), the tip of the giant branch (TRGB) or the host-galaxy recession velocity corrected for the Virgo infall (HF). See Section 5 for details and references.
[b]Obtained from the literature, except for SNe 2007sr, 2007on and 2009ab (Stritzinger et al., in preparation). For these three SNe, $\Delta m_{15}(B)$ estimates were obtained using the multicolour template light curve fitter SNooPy (Burns et al. 2011).
[c]The values at the maximum brightness. Corrected for Galactic extinction.
[d]References for the photometric properties. A05: Anupama, Sahu & Jose (2005); A07: Altavilla et al. (2007); B03: Branch et al. (2003); B04: Benetti et al. (2004); C01: Cappellaro et al. (2001); C03: Candia et al. (2003); G96: Gómez, López & Sánchez (1996); H00: Hernandez et al. (2000); J99: Jha et al. (1999); K03: Krisciunas et al. (2003); K05: Kotak et al. (2005); L98: Lira et al. (1998); L01: Li et al. (2001); L07: Leonard (2007); L09: Leloudas et al. (2009); M05: Mattila et al. (2005); M10b: Maeda et al. (2010b); P96: Patat et al. (1996); P04: Pignata et al. (2004); P07a: Pastorello et al. (2007a); P07b: Pastorello et al. (2007b); P08: Pignata et al. (2008); R95: Richmond et al. (1995); R99: Riess et al. (1999); R05: Reindl et al. (2005); S04: Sollerman et al. (2004); S05: Stehle et al. (2005); S07: Stanishev et al. (2007); S10a: Stritzinger et al. (2010); S10b: Stritzinger et al. (in preparation); W08: Wang et al. (2008); W09: Wang et al. (2009a); and Y09: Yamanaka et al. (2009).
[e]References for the late-time spectra.
[f]An SBF distance to NGC 3226, a member of the same group.

study is listed in Table 1. Their late-time spectra in the wavelength range covering [Fe II] and [Ni II] are shown in Fig. 1. Details on SN 2006dd are presented in Stritzinger et al. (2010), while that on SNe 2007on, 2007sr and 2009ab will be presented elsewhere.

M10a measured the wavelength shifts in [Ni II] λ7378 at late phases for the majority of the SNe Ia listed in Table 1. In M10b, they also measured the shift in [Fe II] λ7155. In this study, we remeasured these line shifts and updated the velocity shift ($v_{\rm neb}$) as follows: when both [Ni II] λ7378 and [Fe II] λ7155 were identified, we fitted their central wavelengths with Gaussian profiles simultaneously using the IRAF deblend command.[5] $v_{\rm neb}$ is taken to be the mean value of them (see also M10b).[6] As a default estimate, the continuum is taken to be constant across the wavelength range. We estimated the error in the fit by varying the continuum. We further considered the errors arising from the difference in the velocity shifts of the two lines. The regions emitting these two lines are not exactly the same since the region emitting [Ni II] λ7378 is attributed to be a product of the deflagration at the very beginning, while that emitting [Fe II] λ7155 is a product from a later phase, but still before the ignition of the detonation (M10a; see also M10c for an example of a detailed nucleosynthesis study). Therefore, there could be intrinsic differences in the velocity shifts of these two lines. The final error bars are taken to be the larger one between the errors associated with the Gaussian fit and the difference in the two lines.

In the majority of SNe, the shifts seen in [Ni II] λ7378 agree with those measured in [Fe II] λ7155 to within an error of at most ~600 km s^{-1}. If only one of these lines could be identified, we estimated the velocity shift only from the single line using the (single-line) Gaussian fitting command within IRAF and assumed that the error is 600 km s^{-1}. In the case of the fast-declining 1986G-like SN 2007on (Morrell et al. 2007) and the peculiar (in terms of the late-time spectra) SN 2004dt (M10b), we did not use the [Ni II] feature as it might be contaminated or originate from [Ca II] λλ7291, 7324 (Filippenko et al. 1992; Turatto et al. 1996). Indeed, we suspected that [Ca II] λλ7291, 7324 might contribute much to the '[Ni II] feature' for SNe 1994D, 2003hv, 2004dt and 2007on, since the measured position of the [Ni II] feature is close to the rest

[5] IRAF is distributed by the National Optical Astronomy Observatories, which are operated by the Association of Universities for Research in Astronomy, Inc., under cooperative agreement with the National Science Foundation.
[6] The two lines were not simultaneously fitted in the previous measurements and this changed the exact values of $v_{\rm neb}$. However, the old and new measurements are mostly consistent within the associated errors. The only exception is SN 1990N, for which the host galaxy redshift was incorrectly treated in the previous measurement. We confirmed that the conclusions of M10a and M10b are not affected by the difference in the measurement in $v_{\rm neb}$.

wavelength of the [Ca II]. Among these SNe, we regard that the [Ni II] identification is the case for SNe 1994D and 2003hv, since its velocity shift agrees with that measured from the [Fe II]. On the other hand, these velocities are inconsistent for SNe 2004dt and 2007on; thus, we believe that [Ca II] is a more likely identification for these two SNe. This indicates that the strong [Ca II] in the late phase may be a property shared by a part of fast-declining SNe and related objects, but not by Branch-normal SNe. When spectra at several epochs were available, we adopted $v_{\rm neb}$ estimated from the latest epoch for which the quality of the spectrum was sufficiently high, since a more secure estimate of the intrinsic velocity shift for the nebular emission lines is possible using later-phase data (Section 2). As shown in Fig. 2, $v_{\rm neb}$ measured for the same SN at different epochs agrees within the errors, at least for $\gtrsim$150 d.

4 INTRINSIC COLOUR VARIATIONS

We first examine whether the intrinsic colours of SNe Ia are related to $v_{\rm neb}$ and therefore to the viewing direction of an observer in the asymmetric explosion scenario. For this purpose, we define the *pseudo-colour* ($B_{\rm max} - V_{\rm max}$) as the difference between the peak B and V magnitudes obtained at the time of the maximum light *in each bandpass*.

We first identify a 'low-extinction' sample of SNe for which the extinction within the host galaxy is likely insignificant. We regard SNe as low extinguished if (i) the host is an elliptical or S0 galaxy; or (ii) the SN was located in the outskirts, farther from the centre than half of the apparent radius of the host (defined as the length of the projected major-axis at the isophotal level 25 mag arcsec^{-2}; Paturel et al. 1991) as obtained from the Lyon-Meudon Extragalactic Data base (Paturel et al. 2003). We also remove SN 2000cx, since this was reported to show peculiar colours (Li et al. 2001; Candia et al. 2003). Our adopted 'low-extinction' sample then comprises 11 objects.

It has been shown that the colours of SNe Ia at the maximum brightness are related to $\Delta m_{15}(B)$ such that SNe with a larger decline rate are intrinsically redder (e.g. Phillips et al. 1999). Fig. 3 shows

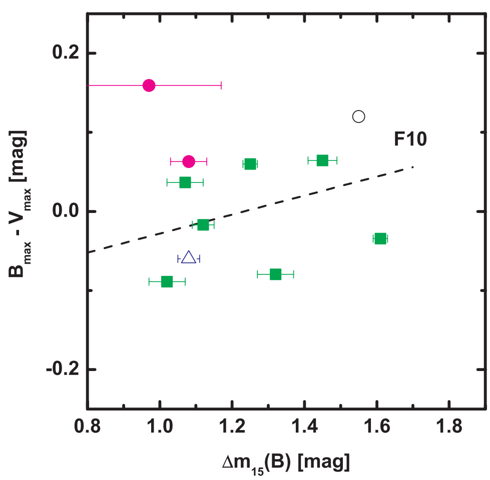

Figure 3. The $B_{\rm max} - V_{\rm max}$ colour of 11 'low-extinction' SNe as a function of $\Delta m_{15}(B)$. The colour is corrected for the Galactic extinction only. SNe are shown by different symbols defined as follows: LVG SNe by the green filled squares, HVG SNe by the magenta filled circles and the fast-declining SN 2007on by a black open circle. SN 2006dd, for which no information on its velocity gradient is available, is shown by a blue open triangle. The relation between colour and $\Delta m_{15}(B)$ as derived by F10 is shown by a dashed line.

a comparison between $\Delta m_{15}(B)$ and the pseudo-colour ($B_{\rm max} - V_{\rm max}$) for our low-reddening sample, corrected for Galactic extinction adopting the values derived from the dust maps of Schlegel, Finkbeiner & Davis (1998) and $R_V = 3.1$. Following the suggestion by M10b that the viewing direction is related to the velocity gradient, we hereinafter plot the SNe with different symbols depending on whether they belong to the LVG or the HVG group. Although we do not see a strong correlation, our data are overall consistent with the $\Delta m_{15}(B)$–colour relation of the 'low-reddened' sample of F10 defined as $c(\Delta m_{15}(B)) \equiv (B_{\rm max} - V_{\rm max})_0 = -0.016 + 0.12[\Delta m_{15}(B) - 1.1]$ mag.

Fig. 4 shows a comparison between $v_{\rm neb}$ and pseudo-colour corrected for the Galactic extinction *and* the colour versus $\Delta m_{15}(B)$ relation of F10. In other words, we are investigating a relation between $v_{\rm neb}$ and the 'colour residual' after correcting for the $\Delta m_{15}(B)$ term. Fig. 4 reveals that there is a clear correlation between $v_{\rm neb}$ and this colour for the low-extinction sample. A linear fit to the 11 SNe results in a chance probability of only 4.4×10^{-4} (i.e. 3.3σ significance). The standard deviation is 0.05 mag. Fig. 4 further shows that almost the same relation applies even when not restricted to the low-extinction SNe (but omitting three evidently highly reddened SNe). This suggests that the $v_{\rm neb}$–colour relation is at least as important as the $\Delta m_{15}(B)$ correction in the colour. It further indicates that a large part of the colour variations of SNe Ia can be attributed to intrinsic variations due to different viewing directions, rather than the host extinction. The intrinsic colour we derive can be expressed by the following equation:

$$(B_{\rm max} - V_{\rm max})_0 = 0.016 + 0.12[\Delta m_{15}(B) - 1.1] + 0.047(v_{\rm neb}/1000\ {\rm km\ s^{-1}})\ {\rm mag}. \quad (1)$$

It has been suggested that some HVG SNe may be intrinsically redder than LVG SNe (e.g. Pignata et al. 2008). Wang et al. (2009b) showed that SNe with higher Si II absorption velocity (which is a typical signature of HVG SNe) are intrinsically redder than those with lower velocity (roughly corresponding to LVG SNe) by ~0.1 mag. Therefore, we qualitatively expect that SNe with larger (positive) $v_{\rm neb}$ are intrinsically redder according to M10b, which is consistent with the data shown here. This also explains why Wang et al. (2009b) obtained a smaller dispersion in the calibrated luminosities by assuming a smaller R_V for SNe with higher velocity in the Si II absorption (i.e. roughly equivalent to that of HVG SNe). If these SNe are intrinsically redder than the others, then a smaller R_V mimics the effect of the viewing direction.

Fig. 5 shows a comparison between the velocity gradient and $B_{\rm max} - V_{\rm max}$ [corrected for Galactic extinction and the $\Delta m_{15}(B)$ term]. As suggested previously, HVG SNe are redder than LVG SNe. The linear fit results in $P = 0.0073$ (2.4σ) for the low-reddened SNe. We note that the distribution can actually be better expressed by a bimodal distribution (HVG SNe and LVG SNe) rather than a continuous distribution. Velocity gradients are similar for all LVG SNe, whereas we can see a colour variation as a function of $v_{\rm neb}$ also within this group. The correlation with the velocity gradient is indeed weaker than the relation using $v_{\rm neb}$. This suggests that $v_{\rm neb}$ is a better indicator of the intrinsic colour than the velocity gradient. This mostly stems from the saturation of the velocity gradients for LVG SNe, which makes it difficult to derive the detailed viewing direction directly from the velocity gradient (M10b).

Our finding that the colour is strongly correlated with $v_{\rm neb}$ suggests that the viewing direction is indeed an important property which controls the colour as theoretically investigated by Kasen et al. (2009) (see also Foley & Kasen 2011). M10b attributed the

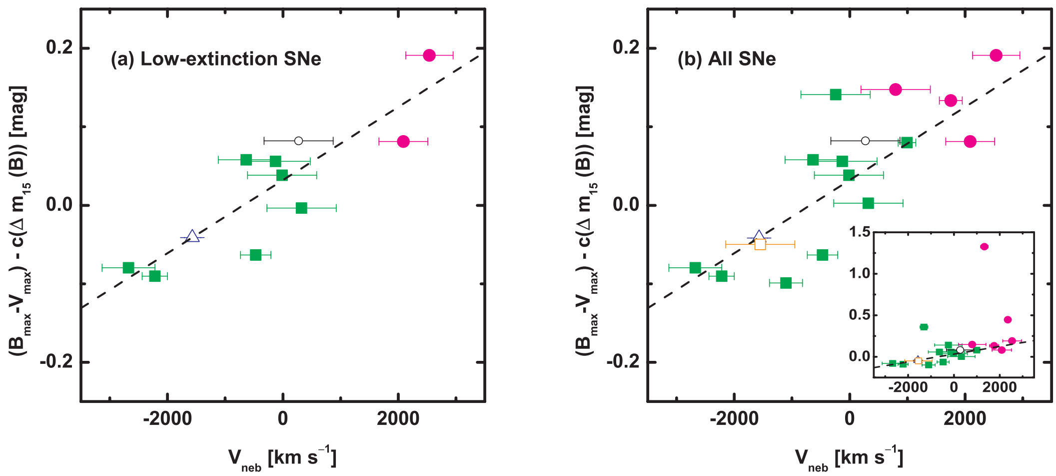

Figure 4. The $B_{\rm max} - V_{\rm max}$ colour, *after* correction of the $\Delta m_{15}(B)$–colour relation of F10 [$c(\Delta m_{15}(B))$: see the main text], versus $v_{\rm neb}$. The dashed line is the best linear fit to the 11 low-extinction SNe. Panel (a) shows the low-extinction sample and panel (b) shows the entire sample (zoomed in the same region as in panel a). The inset in panel (b) shows the entire sample, including also the three highly reddened SNe Ia. SNe are shown by different symbols defined as follows: LVG SNe by the green filled squares, HVG SNe by the magenta filled circles and the fast-declining SN 2007on by a black open circle. SN 2004dt, which was suggested to be a peculiar outlier based on its late-time spectrum, is shown by an orange open square. SN 2006dd, for which no information on its velocity gradient is available, is shown by a blue open triangle.

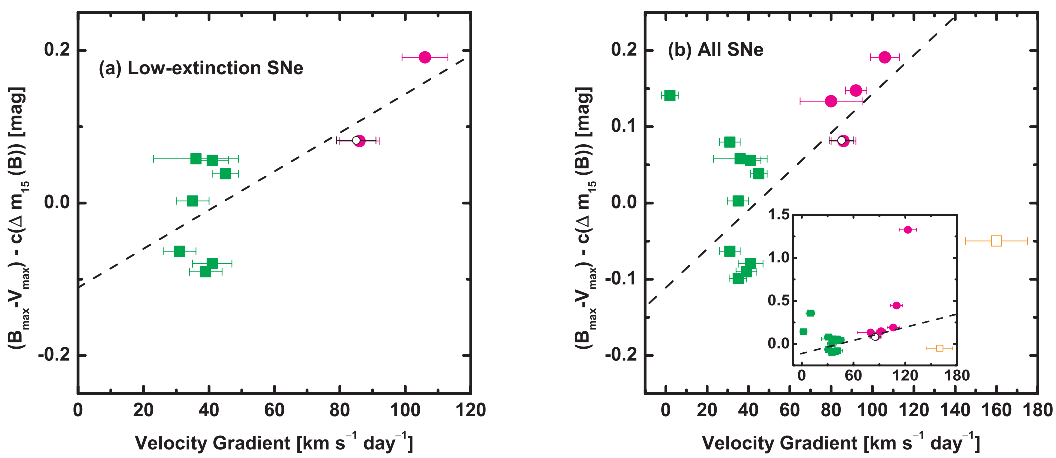

Figure 5. The $B_{\rm max} - V_{\rm max}$ colour, *after* the correction of the $\Delta m_{15}(B)$–colour relation of F10 [$c(\Delta m_{15}(B))$; see the main text], as a function of the velocity gradient $\dot{v}_{\rm Si}$. The dashed line is the best linear fit to the 10 low-extinction SNe (excluding SN 2006dd for which the velocity gradient is not available). The symbols and colour coding indicate the velocity gradient near the maximum brightness (see the caption for Fig. 4).

variation in velocity gradients to different radial density distributions at different directions; they suggested that the photospheric velocity is smaller and evolves more slowly for a direction closer to the offset ignition direction. A smaller photospheric velocity ($v_{\rm ph}$) leads to a larger photospheric temperature ($T_{\rm eff}$) since $T_{\rm eff} \propto v_{\rm ph}^{-1/2}$. The larger $T_{\rm eff}$ results in a bluer colour (cf. figs 1 and 3 of Nugent et al. 1995). Also, the difference in $T_{\rm eff}$ has been suggested to be a main origin of different spectral features seen in HVG and LVG SNe (Hachinger et al. 2008; Tanaka et al. 2008). This qualitatively explains the tendency we have identified in the data.

This result opens up a possibility to estimate the host extinction by including the effect of the viewing angle on different SNe: we compute the colour excess due to the host extinction as $E(B - V) \equiv (B_{\rm max} - V_{\rm max}) - (B_{\rm max} - V_{\rm max})_0$, where the SN intrinsic colour $(B_{\rm max} - V_{\rm max})_0$ is expressed by equation (1). Note that some SNe then show small negative colour excesses, since equation (1) expresses the mean behaviour of the low-extinction SNe with the standard deviation of $\sim$0.05 mag. We have used this method to estimate the extinction within the host or the environment around the SN and have tabulated our results in Table 2.

We then compare the derived colour excesses to those previously estimated in the literature. We focus on a comparison with $E(B - V)$ computed by Wang et al. (2009b), since these were derived in a homogeneous and systematic way (and there is a sufficient overlap with our samples), but in Appendix A we also compare our values with other estimates of $E(B - V)$ found in the literature (reaching the same qualitative conclusion). Fig. 6 shows a comparison between $E(B - V)$ as derived in this study and the values from Wang et al. (2009b), for 16 SNe which are common in the two studies. Fig. 6 shows that the colour excess we derived tends to be smaller, since a large part of the colour variation is interpreted to reflect the intrinsic colour variation rather than the host extinction. Indeed, the slope between the two estimates is consistent with $\sim$3/1.85 for objects with $E(B - V) \lesssim 0.2$, where 1.85 is the value of R_V obtained by Wang et al. (2009b) for their whole sample. This means that even if we assume $R_V \sim 3$ to convert our $E(B - V)$ estimate to A_V, the

Table 2. $E(B-V)$.

SN	$\Delta m_{15}(B)$ correction[a] (mag)	$v_{\rm neb}$ correction[b] (mag)
1990N	0.056	0.030
1994D	−0.090	−0.019
1997bp	0.19	0.041
1998aq	−0.099	−0.079
1998bu	0.36	0.39
2000cx	0.14	0.12
2001el	0.080	0.002
2002bo	0.45	0.30
2002dj	0.081	−0.048
2002er	0.15	0.078
2003du	−0.063	−0.073
2003hv	−0.080	0.013
2004dt	−0.050	−0.010
2004eo	0.038	0.007
2005cf	0.003	−0.045
2006X	1.33	1.23
2006dd	−0.042	0.000
2007on	0.082	0.037
2007sr	0.13	0.020
2009ab	0.058	0.056

[a]Corrected for the colour–$\Delta m_{15}(B)$ relation of F10.
[b]Corrected for the colour–$\Delta m_{15}(B)$ relation *and* the colour–$v_{\rm neb}$ relation (equation 1).

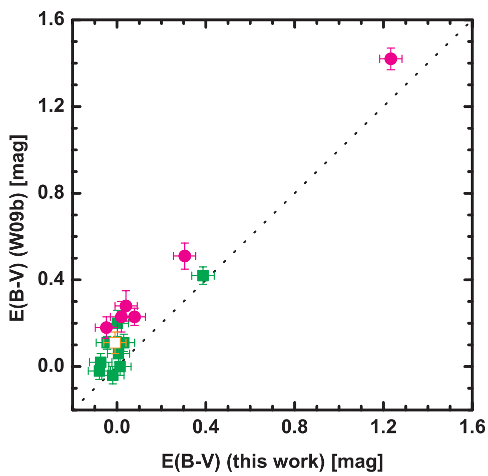

Figure 6. Comparison of the extinction. The horizontal axis denotes the values of $E(B-V)$ derived in this study corrected for $v_{\rm neb}$ (Table 2), while the vertical axis provides values from Wang et al. (2009b). The comparison is shown for 16 SNe which are common between the two studies. The symbols and colour coding indicate the velocity gradient near the maximum brightness (see the caption of Fig. 4).

extinctions we derive are mostly consistent with those derived by the other method. Exceptions are the heavily reddened SNe, especially SN 2006X. This means that at least part of the reason why a small R_V is preferred for the luminosity standardization might be attributed to an overestimate of the host extinction (F10), although at least SN 2006X clearly requires small R_V.

5 COMPUTING INTRINSIC LUMINOSITIES AND RESIDUALS OF TYPE Ia SNe

To investigate any residuals in the intrinsic luminosities of SNe Ia, it is crucial that the distance to each event is estimated carefully. The distance should be provided independently of the SN properties. Most of the SNe Ia in our sample are nearby (that is why late-time spectral observations were possible for these objects) and therefore the most-accurate distance estimates to their host galaxies come from direct distance measurements such as Cepheid variables or the surface brightness fluctuation (SBF) method. Although the Cepheid measurements, available for four SNe in our list, are regarded as the most-reliable estimates, there is disagreement in different analyses of the Cepheid data. The Cepheid distance measurements have mainly been contributed by the Saha–Tammann–Sandage SN Ia Hubble Space Telescope Calibration Program (hereinafter STS, Saha et al. 2006) and by the HST key project (hereinafter KP: Freedman et al. 2001; Stetson & Gibson 2001). The KP distances are typically shorter by 0.2–0.3 mag than those of the STS (see Riess et al. 2005; Wang et al. 2006, for a discussion). Unfortunately, such a systematic difference is important for our study, since it is exactly the order of magnitude of the effect we hope to investigate. We have chosen to adopt the KP distances since they have been suggested to give smaller dispersion in the residuals (e.g. Wang et al. 2006) and since this is the distance scale the SBF distances have been calibrated to (see below). In Appendix B, we discuss how our results would be modified if we instead had adopted the STS distances.

In the case of the SBF measurements, we used the values given by Tonry et al. (2001) and included the 0.16-mag correction suggested by Jensen et al. (2003) to fit to the KP Cepheid zero-point. For the SN host galaxies not listed in Tonry et al. (2001), we used values given by Ajhar et al. (2001) in which the zero-point is calibrated in a similar manner.

There are several objects which require additional considerations about the distance:

(i) For SN 2000cx in NGC 524, an SBF distance of $\mu = 31.74 \pm 0.20$ mag is available. However, this value is significantly smaller than the Hubble flow (HF) distance (see below) of 32.63 ± 0.27 mag. We suspect that the SBF distance to NGC 524 is not correct and have decided to adopt the HF distance for this SN (see also Appendix B).

(ii) Neither a Cepheid nor an SBF distance is available for SN 2001el. We therefore used a distance based on the NIR Tully–Fisher relation (Willick et al. 1997).

(iii) For SN 2002bo, direct distance measurements are not available. However, there are SBF distances measured for two possible members of the group (see Krisciunas et al. 2004): NGC 3193 ($\mu = 32.50 \pm 0.18$ mag) and NGC 3226 (31.70 ± 0.24 mag), which, however, do not agree with each other. The latter value is consistent with the HF distance (31.44 ± 0.48 mag) and we have therefore decided to adopt the latter SBF value.

(iv) For SN 2006dd, Feldmeier, Jacoby & Phillips (2007) reported a distance to NGC 1316 based on the planetary nebula luminosity function (PNLF) as $\mu = 31.26 \pm 0.10$ mag, which Stritzinger et al. (2010) argued is more reliable than the SBF distance (31.50 ± 0.17 mag). Therefore, we adopt the PNLF distance in this paper.

(v) In the case of SN 2007sr, Schweizer et al. (2008) reanalysed *Hubble Space Telescope* data used by Saviane et al. (2008) and obtained a tip of the red giant branch distance of $\mu = 31.51 \pm 0.17$ mag, which is in agreement with the HF distance. We adopt this value as the distance to SN 2007sr.

Finally, there are a number of events for which we had to rely on the HF distance-scale, since estimates based on the aforementioned methods are not available. Recession velocities were corrected for the Virgo infall as obtained from the Lyon-Meudon Extragalactic Data base (Paturel et al. 2003) and converted to a distance modulus using $H_0 = 72\,\mathrm{km\,s^{-1}\,Mpc^{-1}}$ (Freedman et al. 2001). The correction with respect to the heliocentric radial velocity due to the Virgo infall is typically less than $100\,\mathrm{km\,s^{-1}}$. In these calculations, we assumed an uncertainty of $300\,\mathrm{km\,s^{-1}}$ to account for peculiar motions.

Reddening due to dust is the other main problem to estimate the SN luminosity. Although we suggest that a large part of the colour variation is intrinsic at least if we omit highly reddened SNe (Section 4), the corrected colour excesses are not always negligible (Table 2). For Galactic extinction, we adopt the dust maps of Schlegel et al. (1998) with $R_V = 3.1$. We have estimated the host extinction using the method developed and described in Section 4 (see equation 1). The associated $E(B-V)$ colour excess (Table 2) was then converted to A_V using the relation $A_V = R_V E(B-V)$. The associated error is

$$\sigma_{A_V}^2 = R_V^2 \sigma_{E(B-V)}^2 + [E(B-V)]^2 \sigma_{R_V}^2. \quad (2)$$

Estimating the uncertainty in R_V is not trivial. We have assumed the typical value derived by F10, that is, $\sigma_{R_V} = 0.3$. Following the procedure of the previous section, we adopted an error of 0.05 mag for $E(B-V)$. We assumed $R_V = 1.72$ since to derive the residuals we used the light-curve correction from F10, who obtained this value as the best-fitting parameter. In Appendix B, the effect of the uncertainty in R_V upon our results is further investigated.

We note that there are two approaches in treating the colour and extinction for SNe Ia (see e.g. F10 for further discussion). In one approach, the colour and the light-curve shape are simultaneously varied to obtain the standardized luminosity (e.g. Guy et al. 2007). In the other approach, first the intrinsic colour is associated with other observed parameter(s) [e.g. $\Delta m_{15}(B)$] and any excess beyond this colour is assumed to be caused by the host extinction (e.g. Phillips et al. 1999). We follow the latter approach in this paper. We, however, emphasize that our treatment takes into account the intrinsic colour variations, independent of $\Delta m_{15}(B)$, as is done in the former, simultaneous-fitting approach.

The observed V-band peak magnitude was converted to the absolute peak magnitude (M_V) using the distance modulus and the extinction as described above. We have not included K-corrections, since the correction is at most ~0.01 mag at the maximum brightness for SNe at the low redshifts considered here (Hamuy et al. 1993; Nugent, Kim & Perlmutter 2002). For the residual, the difference between the absolute peak V magnitude (M_V) and the standardized magnitude predicted by the Phillips relation [$\bar{M}_V(\Delta m_{15}(B))$] was computed. In obtaining the 'standardized' peak magnitude, we applied an updated relation presented by F10 (see their table 9.). Hereinafter, we denote the residual by $\mathrm{d}m \equiv M_V - \bar{M}_V(\Delta m_{15}(B))$. Table 3 summarizes the M_V values that we computed, along with the standardized peak magnitudes. Also shown are the estimated errors in the calibration.

In the resulting distribution of M_V, the dispersion is at the level of ~0.28 mag. This value is larger than that typically derived from samples of SNe Ia (~0.1–0.2 mag; e.g. F10). We note, however, that such studies make use of uniform data sets and minimize the dispersion by parameter fitting the entire data set, including the simultaneous fit to the light-curve shape [e.g. $\Delta m_{15}(B)$] and colour (i.e. R_V and intrinsic SN colour). Given that we have compiled data from various sources and adopted an external relation (F10) derived from an independent data set, a larger dispersion is expected. More importantly, most of the SNe Ia in our analysis are nearby and are not in the smooth HF, so that the uncertainty in the distance estimates is larger (due to peculiar velocities; see e.g. fig. 19 of F10).

Table 3. Peak luminosity calibration.

SN	$\bar{M}_V(\Delta m_{15}(B))$ (mag)	M_V (mag)	dm (mag)	$\sigma^a_{A_V}$ (mag)	$\sigma^b_{M_V}$ (mag)
1990N	−19.15	−19.14	0.01	0.087	0.17
1994D	−18.91	−19.12	−0.21	0.086	0.22
1997bp	−19.24	−18.97	0.27	0.087	0.28
1998aq	−19.10	−19.01	0.09	0.089	0.12
1998bu	−19.16	−18.97	0.19	0.14	0.25
2000cx	−19.28	−19.85	−0.57	0.093	0.29
2001el	−19.09	−18.55	0.54	0.086	0.46
2002bo	−19.06	−18.72	0.34	0.13	0.27
2002dj	−19.14	−18.89	0.25	0.087	0.26
2002er	−18.91	−18.91	0.00	0.089	0.27
2003du	−19.20	−18.76	0.44	0.089	0.31
2003hv	−18.64	−18.90	−0.26	0.086	0.31
2004dt	−19.02	−19.28	−0.26	0.086	0.15
2004eo	−18.79	−19.11	−0.32	0.086	0.16
2005cf	−19.10	−18.84	0.26	0.087	0.34
2006X	−18.92	−19.07	−0.15	0.38	0.43
2006dd	−19.14	−18.94	0.20	0.086	0.13
2007on	−18.69	−18.54	0.15	0.087	0.21
2007sr	−19.12	−19.01	0.11	0.086	0.19
2009ab	−18.98	−18.79	0.19	0.088	0.22

[a] Error in the extinction estimate.
[b] Total error including the extinction and distance uncertainties.

6 RELATION BETWEEN THE LATE-TIME EMISSION-LINE SHIFT AND THE LUMINOSITY RESIDUALS

In this section, we explore whether there are any relations between v_{neb} and the luminosity of SNe Ia at the maximum brightness. We have first investigated whether v_{neb} correlates with the absolute magnitude M_V. In Fig. 7, it is shown that there is no apparent correlation between these two parameters. The observed distribution of M_V as a function of v_{neb} can emerge from a non-correlation at the 14 per cent level ($P = 0.14$), as derived by our Monte Carlo simulations (see Appendix C). There is a clear outlier in the plot,

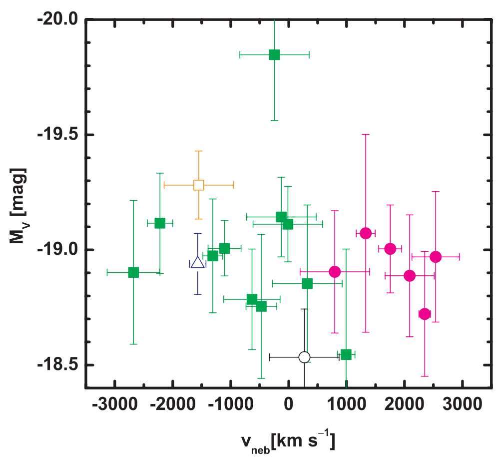

Figure 7. M_V as a function of v_{neb}. The symbols and colour-coding indicate the velocity gradient near the maximum brightness (see Fig. 4 caption).

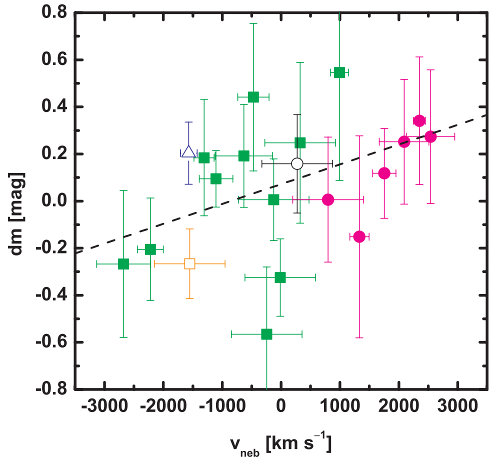

Figure 8. The residuals dm as a function of $v_{\rm neb}$ (see Fig. 4 caption). The black dashed line shows the best linear fit to the entire data set (Table 4).

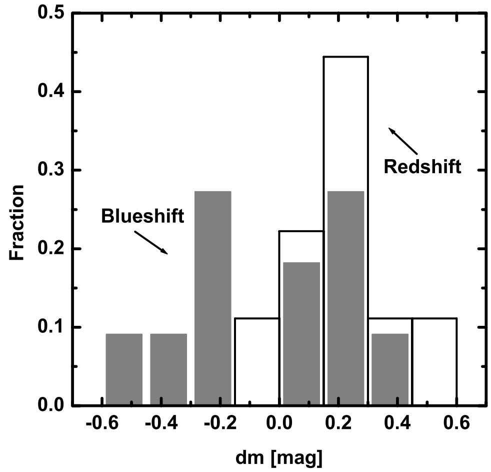

Figure 9. Fractional number distribution of the 20 SNe Ia as a function of dm. SNe Ia are divided into two categories: those showing a blueshift in the late-time emission lines (grey) and those showing a redshift (white).

Table 4. Relations between $v_{\rm neb}$ and dm.

Sample	N^a	α^b	β	P^c	Significance
All	20	0.084 ± 0.051	0.072 ± 0.077	0.053	1.6σ
'Bright'[d]	10	0.028 ± 0.071	0.12 ± 0.10	0.35	0.4σ
'Faint'[e]	10	0.13 ± 0.079	0.056 ± 0.13	0.054	1.6σ

[a]Number of SNe.
[b]The best fit using the relation d$m = \alpha(v_{\rm neb}/1000\,{\rm km\,s^{-1}}) + \beta$. The errors for α and β are 1σ.
[c]Probability that the distribution arises from a non-correlation.
[d]SNe with $\Delta m_{15}(B) \le 1.12$.
[e]SNe with $\Delta m_{15}(B) \ge 1.13$.

that is, SN 2000cx (see also Li et al. 2001). Even if we omit this single SN from the fit, the fitting result is not improved ($P = 0.19$).

In the next step, we investigated if $v_{\rm neb}$ correlates with the luminosity residual dm (Fig. 8). According to the Monte Carlo simulations (see Appendix C), these two quantities are correlated at the 1.6σ level. The best linear fit to the 20 data points, expressed by d$m = \alpha(v_{\rm neb}/1000\,{\rm km\,s^{-1}}) + \beta$, is given in Table 4. We note that this investigation is limited by the relatively large errors in dm associated with the distance uncertainties to the SNe (Section 5 and Appendix B). If we arbitrarily choose to ignore these errors (that were computed with a range of different methods) and consider only the errors associated with the extinction (that were derived in a systematic way), we observe that the significance of the proposed correlation increases (2.4σ; $P = 0.0092$). Although the significance for the observed correlation is low, it deserves further study when a larger sample is available.

There may be a concern that the apparent relation in the $v_{\rm neb}$ – dm could be dominated by single points, rather than expressing a general trend. To examine this, we artificially removed single points from the data set and determined how much the quality of the fit was affected. We thereby obtained $P = (0.038–0.086)$ (1.4σ–1.8σ), depending on which of the 20 points was removed. Also, the resulting fits were all consistent within the 1σ error.

We also split the SN sample into halves according to the value of $\Delta m_{15}(B)$ and repeated the fitting for both subsamples (Table 4). We find that the 'faint' group [with $\Delta m_{15}(B) \ge 1.13$ mag[7]] shows a correlation with a significance similar to that using the entire sample. On the other hand, the correlation is not evident for 'bright' SNe with $\Delta m_{15}(B) \le 1.12$. We note that the best-fitting slope for the faint sample is steeper than the one for the entire sample, as expected from the behaviour of the bright sample. A possible interpretation is presented in Section 7.

We have also investigated a tendency by dividing the sample depending on $v_{\rm neb}$. Fig. 9 shows the number fraction of SNe Ia as a function of dm. In this figure, the subsamples with $v_{\rm neb} < 0$ (blueshift) and that with $v_{\rm neb} > 0$ (redshift) are marked differently. Fig. 9 shows that there is a tendency that SNe Ia having blueshifts/redshifts in the late-time emission lines are brighter/fainter than expected from the Phillips relation.

The difference between the average values for dm in the 'blueshift' group ($N = 11$) and 'redshift' group ($N = 9$) is ∼0.25 mag. To examine the statistical significance, we performed Monte Carlo simulations as follows. First, we randomly selected 11 out of the 20 SNe ('A group') and then the remaining nine SNe were labelled as 'B group'. We then calculated the difference between the average values of dm in the two groups. With 10^5 Monte Carlo realizations, we find that the probability, P, that dm (A) − dm (B) $\lesssim -0.25$ mag is $P = 0.023$ (2.0σ).

7 A TOY MODEL FOR THE VIEWING ANGLE EFFECTS

In the off-centre asymmetric SN Ia explosion scenario (Section 2), a correlation between $v_{\rm neb}$ and dm is expected. The viewing angle effect on the peak brightness has been investigated by several authors. Sim et al. (2007) considered kinematic models for an off-centre distribution of ^{56}Ni, computed the radiation transfer in 2D and showed that the luminosity can be different by ∼0.5–1.5 mag for an observer at the offset direction as compared to the opposite direction. More recently, Kasen et al. (2009) investigated a series of off-centre hydrodynamic models in 2D, in which the deflagration was ignited in an off-centre manner (see also M10c), obtaining peak magnitude differences at the level of ∼0.5 mag for different viewing angles. There is also an expectation that the colour is affected by the viewing angles, as investigated by Kasen et al. (2009) and Foley & Kasen (2011). However, there was no strong observational hint on the geometry of the inner ejecta at the time of their publications

[7] Here the dividing value, $\Delta m_{15}(B) = 1.13$, is set merely by the requirement to split the sample into halves.

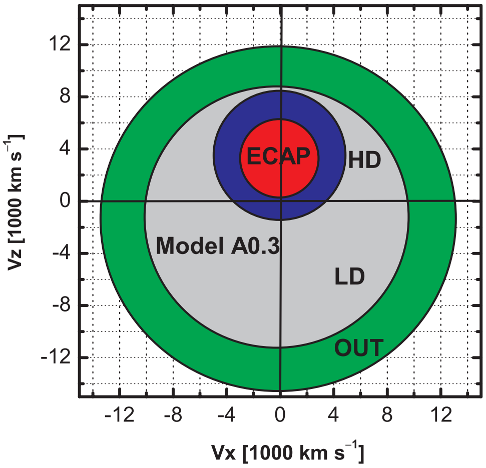

Figure 10. The toy model used for the light-curve calculations. The structure of the ECAP and HD zones is directly taken from the model of SN 2003hv (M10a).

(but see Foley & Kasen 2011). In addition, they did not discuss the outcome of the off-centre ignition at the late phases as was investigated by M10ab. In the following, we investigate the effect of the viewing angle on the peak luminosity and colour, adopting the simple explosion geometry proposed by M10ab.

In the toy model shown in Fig. 10, the innermost regions are divided into two characteristic zones: a zone dominated by neutron-rich Fe-peak elements produced by electron captures [Electron-CAPture (ECAP)], the relatively high density ^{56}Ni-rich region surrounding the ECAP region [High-Density (HD)] and then the outer, relatively low density ^{56}Ni-rich region on top of the HD region [Low-Density (LD)]. The ECAP and HD regions are suggested to be responsible for the formation of [Ni II] λ7378 and [Fe II] λ7155, respectively, from which we derived $v_{\rm neb}$. Following M10ab, the ECAP and HD regions have offsets from the centre of 3500 km s^{-1}, whereas the LD region has only a slight offset in the opposite direction. The ECAP and HD zones are interpreted as products of the initial deflagration flame propagation, while the LD zone is a product of the subsequent detonation wave. There is possibly a variation in the offset velocity for different SNe Ia, although in the present analysis we use one specific value (3500 km s^{-1}) as our fiducial model.[8] Note that this distribution was derived by modelling late-time spectra, but it is also qualitatively consistent with the outcome of hydrodynamic models if the deflagration sparks are ignited at an offset (M10c). The hydrodynamic simulations have not yet explored all parameter space, nor been directly compared to observations. We therefore take this 'observationally constrained' toy model as our reference model.

The masses and compositions of the ECAP and HD zones are taken from M10a; the mass of ^{56}Ni is 0.01 M$_\odot$ in the ECAP zone and 0.1 M$_\odot$ in the HD zone. The mass of ^{56}Ni in the LD zone is a parameter, corresponding to the diversity of $M(^{56}{\rm Ni})$ and $\Delta m_{15}(B)$ for various SNe Ia. The radial extent of the LD zone is also taken from M10a. We calculate light curves for models with the total $M(^{56}{\rm Ni})$ from 0.21 to 0.8 M$_\odot$, with 10 per cent increases in $M(^{56}{\rm Ni})$ between models. In the present analysis, we focus on the models with $M(^{56}{\rm Ni}) = 0.3$ M$_\odot$ (roughly consistent with 0.3–0.4 M$_\odot$ derived for SN 2003hv; Leloudas et al. 2009; M10a) and 0.6 M$_\odot$ (for SNe Ia with a typical luminosity; see Stritzinger et al. 2006). We hereinafter refer to the models as A0.3 and A0.6, where the number denotes $M(^{56}{\rm Ni})$. For all the models, the structure in the ECAP and HD zones (i.e. the masses of these zones and the offsets) was assumed to be exactly the same as the one derived for SN 2003hv. We fixed the masses in the ECAP and HD zones since it has been suggested through late-time spectral modelling (Mazzali et al. 2007) that the masses of the innermost region are consistent with no variation for different SNe.

The distribution of elements other than Fe-peak elements was not discussed in M10a, because a large fraction of them are located in the region above the LD zone which is not accessible by late-time observations. These are assumed to be intermediate-mass elements (IMEs) and/or a carbon–oxygen (CO) mixture. We assume an explosion energy of $E_{\rm K} = 1.4 \times 10^{51}$ erg and ejected mass of $M_{\rm ej} = 1.38$ M$_\odot$.[9] These values determine the outermost velocity, as well as the density there. IMEs and CO are assumed to be distributed uniformly in the LD and the outer zones. Accordingly, the mass in the LD zone is the sum of those of ^{56}Ni and IMEs/CO, whereas the outermost zone is purely composed of IMEs or CO.

A question is whether or not the outermost region also shows an offset. To address this, we employ a simple model. It is assumed that the centre of the outer envelope is the same as for the LD zone. This is motivated by the expectation that the outer envelope expansion is caused by the detonation wave. This configuration is roughly consistent with the finding of M10b that SNe viewed from the offset direction (direction of the ECAP zone) are observed as LVG SNe, while those from the opposite direction are HVG SNe because of the existence of a more extended envelope in the direction opposite to the offset. This characteristic is also seen in a hydrodynamic explosion model (see M10b for a detailed discussion).

For different masses of ^{56}Ni, we simulated the bolometric light curve as a function of the viewing angle. The calculations were performed using the Monte Carlo radiation transfer SAMURAI code. SAMURAI is a compilation of 3D codes that adopt Monte Carlo methods to compute high-energy light curves and spectra (Maeda 2006), optical bolometric light curves (Maeda, Mazzali & Nomoto 2006a) and optical spectra from early (Tanaka et al. 2006, 2007) to late phases (Maeda et al. 2006b). For the light curve, the present version allows for a frequency-averaged grey opacity only. The optical transfer scheme follows the prescriptions given by Lucy (2005) (see also Cappellaro et al. 1997). For the opacity to optical photons, we adopted the phenomenological prescription of Mazzali et al. (2001).[10] Because of the simplified kinematic model and the limitations in the light-curve calculations, the following results should be regarded as indicative. A more detailed and quantitative comparison between the model and observations is beyond the scope of this paper.

[8] The presently available data analysed by M10ab are consistent with no variation. To tackle the possible variation in the kinematics and its relation to other explosion parameters would require a larger observational sample.

[9] Strictly speaking, $E_{\rm K}$ is dependent on the final composition. If $M(^{56}{\rm Ni}) = 0.6$ M$_\odot$ and the remaining part is burned into IMEs, then $E_{\rm K} \sim 1.4 \times 10^{51}$ erg. By varying $M(^{56}{\rm Ni})$ between 0.2–0.8 M$_\odot$ and assuming that the remaining fraction is burned into IMEs, the resulting $E_{\rm K}$ is in the range $(1.3–1.5) \times 10^{51}$ erg. Thus, the variation in $E_{\rm K}$ is small and we take $E_{\rm K} = 1.4 \times 10^{51}$ erg as our fiducial value.

[10] We note that the rise time in the models is typically shorter than that estimated by observations. A part of the reason is likely the simplified opacity used in our calculations (see also Sim et al. 2007). As we are only interested in the 'relative' behaviour, for example, differences caused by different viewing angles and by different $M(^{56}{\rm Ni})$, we did not try to obtain better agreement in the rise time.

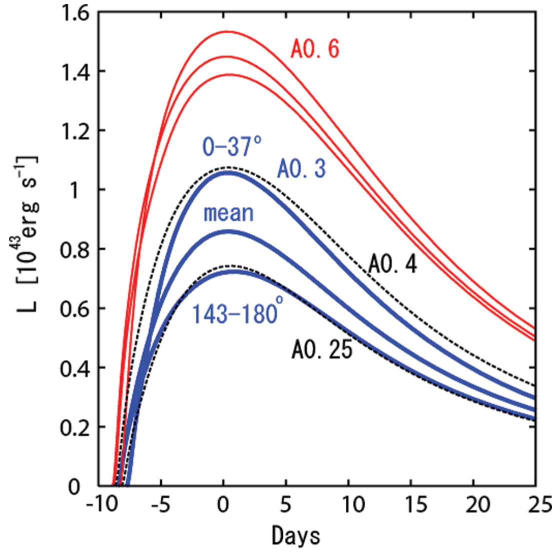

Figure 11. The synthetic bolometric light curves for models A0.3 (blue-thick-solid lines) and A0.6 (red-thin-solid lines). For each model, three curves are shown: two angle-dependent light curves, with the angle measured from the direction of the offset of the ECAP/HD regions, and the mean angle-averaged light curve. For comparison, the mean light curves for models A0.25 and A0.4 are shown (black-dashed lines). Time is defined as days past the bolometric maximum.

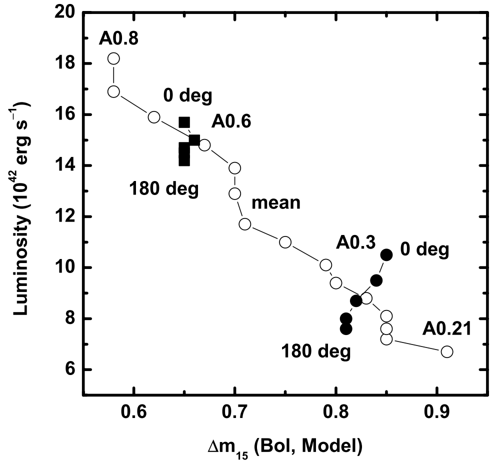

Figure 12. The behaviour of the light-curve shape and the peak luminosity of our models. The horizontal axis denotes Δm_{15} in the synthetic bolometric light curves and the vertical axis denotes the synthetic bolometric luminosity. The open circles denote angle-averaged, mean light curves of different models (from A0.21 to A0.8). The angle-dependent behaviour is shown for models A0.3 and A0.6 by the black filled symbols, where each point stands for the light curve from a certain direction.

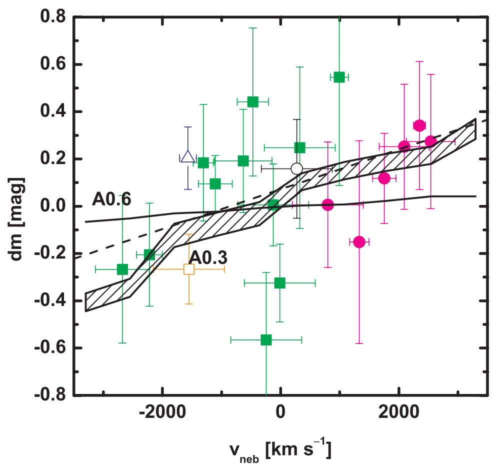

Figure 13. Model results compared to the observed sample in the $v_{\rm neb}$ versus dm diagram. Model A0.3 is shown by the shaded area and model A0.6 is shown by a solid line (see footnote 12). Points are for our sample of SNe and a dashed line is the best linear fit to them (Fig. 8).

Fig. 11 shows the bolometric light curves of models A0.3 and A0.6, for different viewing angles. Model A0.3 shows a difference of ∼30 per cent in the peak luminosity depending on the viewing angle. It is brightest if viewed from the offset direction and faintest from the opposite direction. The reason for this is that photons from the HD zone have lower optical depth in the offset direction and preferentially escape into this direction. On the other hand, the contribution from the nearly spherical LD component is not very sensitive to the viewing angle. In model A0.3, a large fraction of ^{56}Ni (∼30 per cent) is contained in the offset component. The brightness thus depends strongly on the viewing angle. On the other hand, in model A0.6, the contribution of the offset component to $M(^{56}\mathrm{Ni})$ is small (∼15 per cent). Accordingly, the angle dependence is small, at the ∼10 per cent level.

Another important effect is that the light-curve shape can also be different for different viewing angles. Model A0.3 shows that the light curve is narrower and the rise time is shorter if viewed from the direction of the offset, while it is broader and the rise time is longer if viewed from the opposite direction (see also Sim et al. 2007). This stems from the shorter diffusion time-scale in the direction of the offset. Indeed, this effect is part of the reason for the enhancement of the brightness in the offset direction, since a faster rise to the peak results in a larger amount of radioactive γ-rays available to power the peak brightness. The presently available data do not reveal this theoretically expected correlation between $\Delta m_{15}(B)$ and $v_{\rm neb}$ (M10b), although the situation is still consistent with the idea presented here since a large variation in $\Delta m_{15}(B)$ is introduced by different amounts of ^{56}Ni. With an increasing number of nebular spectra, this test will become possible.

The trend in the peak brightness–light-curve width relation arising from different viewing angles works in a way opposite to the Phillips relation (see also Sim et al. 2007). A light curve that is brighter due to asymmetry is also narrower. For example, Fig. 11 shows that the peak brightness of model A0.3 viewed from the offset direction is comparable to the mean (angle-averaged) brightness of model A0.4, while the former results in a narrower light curve. Again, this effect is not as important for model A0.6, for which the light-curve shape does not strongly depend on the viewing direction. Fig. 12 shows the peak luminosity in terms of Δm_{15} as derived from the synthetic bolometric light curves.[11]

Fig. 13 shows the synthetic bolometric magnitude ‘difference’ (∼dm) as a function of $v_{\rm neb}$ (i.e. the viewing angle). It is compared to the V-band residuals as derived in the previous section. Given the uncertainty involved in the comparison (e.g. the simplified ejecta structure), it should be regarded as qualitative.

[11] Note again that our simplified treatment in the opacity and in the ejecta geometry allows us to investigate only the relative behaviour of different models (and viewing directions), but not to directly compare the models and the observational data.

The model behaviour in Fig. 13 was derived through the following procedures. First, we defined a bolometric Phillips relation for the models, based on the angle-averaged, mean light curves in Fig. 12. Then, for a light curve of model A0.3 and *a given viewing direction*, we searched for a 'mean' light curve (spanning model A0.21 to model A0.8) which shows a similar light-curve shape. In general, the considered light curve lies between two mean curves of our model grid.[12] Next, we define the model 'residual' as the magnitude difference between the *angle-dependent* luminosity under consideration and the luminosity of the corresponding mean light curve(s). This procedure is equivalent to deriving the observed residual (d*m*), but with the observed reference light curves replaced by the synthetic 'mean' (angle-averaged) light curves.

To compare the model residual (in bolometric magnitude) and observed residual d*m* (in the *V* band), we have to make one assumption: the *V*-band light curve is (at least qualitatively) traced by the bolometric light curve. Using a sample of SNe with the bolometric luminosity available (Contardo et al. 2000; Stritzinger & Leibundgut 2005), we confirmed that $V_{\rm max}$ is strongly correlated with the bolometric luminosity and that the bolometric correction is not significantly different for different SNe. This justifies our assumption.

In this comparison, not only can the dependence of the peak brightness on the viewing angle be important, but also that of the light-curve shape. For instance, the residual for model A0.3 viewed from the offset direction should be constructed using the mean (angle-averaged) peak brightness of model A0.23 or A0.25, which have similar light-curve shapes to, but smaller luminosity than, model A0.3. A similar argument applies to an observer in the direction opposite to the offset direction. Thus, the resulting model d*m* is generally larger than that estimated by simply taking the difference between the angle-dependent brightness and the mean brightness for the *same model*. For example, the residual for model A0.3 is ~ -0.4 mag if viewed from the offset direction, $\sim +0.3$ mag, if viewed from the opposite direction. Thus, the residual varies by up to ~90 per cent (~0.7 mag) depending on the viewing angle. This is much larger than simply taking the difference between the angle-dependent brightness and the mean brightness for the *same model*, which is ~30 per cent (Fig. 11).

There is a qualitative agreement between the model and the data (Fig. 13). In particular, models with $M(^{56}{\rm Ni}) \sim 0.3\,{\rm M}_\odot$ (model A0.3) agree with the tentative correlation seen in the observed data. Also, if we calculate the expected difference in d*m* for SNe with blueshift (observed at $<90°$) and redshift (observed at $>90°$), taking into account the solid angle, we obtain ~0.4 mag for this model. This is a bit larger than the observed difference between the two groups (Fig. 9 and related discussion), but it explains the observed trend at least qualitatively. Note that the offset velocity has been directly constrained for model A0.3 using SN 2003hv (M10a).

For brighter SNe Ia, model A0.6 predicts a peak brightness almost independent of the viewing angle. We also find that the viewing angle effect on the light-curve shape is not as important for this model. The reason for this is that most of ^{56}Ni is in the 'spherical' LD zone in these models, since the amount of ^{56}Ni in the ECAP and HD zones (the 'offset' region) is fixed. Our analysis of the observational data suggests that the correlation is indeed weaker, as quantified by the correlation slope, for a subset of (brighter) SNe with smaller $\Delta m_{15}(B)$ than for those with larger $\Delta m_{15}(B)$ (see Table 4 and related discussion). This is consistent with the model prediction and may indicate that the contribution from the LD zone is more important and the viewing angle effect less important for brighter SNe. Although we fixed the mass of the offset component in our toy models, there is a theoretical expectation that the mass of the 'offset' region is *smaller* for brighter SNe, since a larger asymmetry results in a weaker deflagration which is then followed by a stronger detonation in the off-centre deflagration-to-detonation transition scenario (Kasen et al. 2009; M10c). This will result in even smaller angle dependence for typical SNe Ia than model A0.6 predicts. A larger sample will be required to clarify the relative contributions from different zones, which in turn will provide hints on the geometry of SNe as a function of $\Delta m_{15}(B)$.

Having computed angle-dependent luminosities, it is now possible to make a crude estimate on the relation between the colour and the viewing direction for our models. The angle-dependent effective temperature is approximately extracted from the model by combining the luminosity and photospheric velocity obtained by integrating the optical depth back inwards along each radial direction (i.e. $T_{\rm eff} \propto v_{\rm ph}^{-1/2} L^{1/4}$, where $v_{\rm ph}$ and the luminosity L are angle-dependent). Then, we convert the effective temperature to the maximum colour $B - V$ assuming a relation between these two obtained for synthetic spectra by Nugent et al. (1995) (see their fig. 3). Since the observational data (Fig. 4) are already corrected for $\Delta m_{15}(B)$, we add a constant to the model $B - V$ colour (i.e. shifted vertically) so that it passes $B - V \sim 0$ at $v_{\rm neb} \sim 0$ (i.e. we focus on the relative colour change depending on the viewing direction). The result is shown in Fig. 14.

Since the model prediction will be sensitive to the assumed outer ejecta structure, this comparison should be regarded to be qualitative. However, this does demonstrate that the basic features in the ejecta structure constrained by the observations (the inner structure from the late-time spectra and the outer structure from the relation between early-time and late-time spectra; M10ab) predict the $v_{\rm neb}$–colour relation found in this paper as well, although the models have not been tuned at all to reproduce this relation. Indeed,

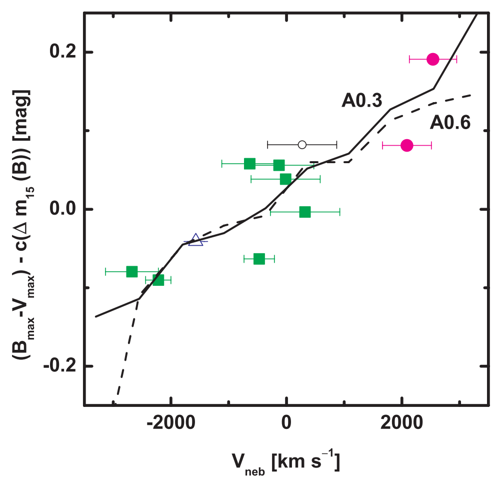

Figure 14. Model results compared to the observed sample in the $v_{\rm neb}$ versus $B_{\rm max} - V_{\rm max}$ diagram (see the main text). Models A0.3 and A0.6 are shown by the solid and dashed lines, respectively. Points are for our low-extinction sample of SNe (Fig. 4a).

[12] For model A0.6, the light-curve shape is not strongly dependent on the viewing direction (Fig. 11). Thus, for model A0.6, the 'model residual' is computed as the magnitude difference between the angle-dependent and mean light curves of the same model A0.6. This is the reason why in Fig. 13 the model residual is expressed by a single line for model A0.6, unlike model A0.3.

Foley & Kasen (2011) have recently reported the same trend in the colour and the viewing direction in their simulation based on a qualitatively similar ejecta structure, independent of this study. The qualitative behaviour, that is, the bluer colour for the direction closer to the offset, stems from the lower expansion velocity, thus higher temperature, in that direction.

Unlike the bolometric luminosity, the relation is insensitive to the mass of ^{56}Ni, since the temperature is only weakly dependent on the luminosity. Under the assumptions within our toy model, the two models – models A0.3 and A0.6 – do predict almost the same relation. This may indeed support why we see in the observations a strong relation in the colour but not in the luminosity residual.

8 DISCUSSION AND CONCLUSIONS

In this paper, we have investigated how the explosion geometry and viewing angle can influence the colour and peak brightness of SNe Ia, and thereby lead to the residuals that remain in the peak magnitudes after application of the light-curve correction. We have used the wavelength shift of late-time emission lines to derive the viewing angle and then compared this quantity with the colour and the luminosity residual for a sample of 20 SNe Ia.

8.1 Intrinsic colour variation

We have found a correlation between the colour at the maximum and the wavelength shift seen in late-time emission lines. Using a subsample of 11 SNe, which likely suffer from insignificant host reddening, selected based on the morphological type of the host galaxy and the position of the SN within the host, we have found that SNe which show a blueshift/redshift in nebular emission lines (i.e. viewed from the offset/antioffset direction in the off-centre ignition scenario) are bluer/redder than expected from the colour–$\Delta m_{15}(B)$ relation. This indicates that the previously suggested colour difference between the 'HVG' SNe and 'LVG' SNe is connected to the viewing direction to the observer.

In the next step, we expanded our sample, including objects with potentially larger host reddening. Except for three very red SNe [$(B_{\rm max} - V_{\rm max}) > 0.2$ mag: SNe 1998bu, 2002bo and 2006X], all other objects agreed well with the colour versus $v_{\rm neb}$ relation derived from the 'low-extinction' sample. This indicates that a significant part of the colour excess previously attributed to the host extinction is actually due to intrinsic colour variations.

This raises the question whether the often preferred value of $R_V \lesssim 2$ (much smaller than the typical Galactic value of ∼3.1) really reflects different properties of interstellar/circumstellar dust around SNe Ia. F10 argued that the optical colour–NIR colour relation can be reproduced even with $R_V \sim 3.2$, once heavily reddened SNe are omitted. On the other hand, they required $R_V \sim 1$–2 to minimize the dispersion in the standardized luminosity calibration. They pointed out that an intrinsic colour variation which does not correlate with the decline rate, but does correlate with the luminosity, may solve this apparent discrepancy. Indeed, the intrinsic variation related to the viewing angle that we have found in this paper does not correlate with the decline rate. If we exclude SNe which are clearly heavily reddened, we see that R_V as large as the Galactic value could be acceptable. This issue requires more careful and systematic analysis based on a larger sample. Also, we note that even if this works for the majority of SNe Ia, some heavily reddened SNe appear to require $R_V \sim 1$–2, as highlighted by SN 2006X (F10).

A toy model constructed with the constraints so that it explains the late-time spectral variation (M10a) and its relation to the early-phase spectral diversity (M10b) predicts the bluer/redder colour for smaller/larger (blueshift/redshift) $v_{\rm neb}$, as is consistent with the observational data. For our model sequence, the predicted trend is not sensitive to $M(^{56}{\rm Ni})$ [or $\Delta m_{15}(B)$].

8.2 Second parameter in the luminosity calibration?

We have also investigated a relation between the SN Ia luminosity residual after calibration with the Phillips relation and the wavelength shift seen in the late-time nebular emission lines. For our small sample, the correlation is not strong and we regard this result as tentative. Keeping this caveat in mind, we see a tendency that SNe Ia with a blueshift/redshift in the nebular lines show a higher/lower peak luminosity than expected by the Phillips relation. There is an average difference of ∼0.25 mag in the peak magnitudes between SNe Ia showing a blueshift and those showing a redshift.

Calculating the light curves based on the geometry derived by M10a for the relatively faint SN Ia 2003hv, we have found that SNe Ia viewed from the offset direction should have a peak brightness larger than the mean and those viewed from the opposite direction should be fainter. The difference between these two extreme observer directions is ∼0.7 mag in our fiducial model A0.3.[13] This behaviour is consistent with the observational data. Also, the averaged difference between SNe showing blueshifts and redshifts is ∼0.4 mag in this model, enough to explain the observed value (∼0.25 mag).

The comparison between SNe Ia with normal/large peak luminosity and the models is less straightforward, since the geometry of such explosions has not been directly constructed from observations. Assuming that the degree of the offset is similar to that of SN 2003hv, we expect that the viewing angle effect is less pronounced for brighter SNe Ia. This is consistent with the behaviour we have found in the data. Further variation is expected since the degree of the offset could be different for SNe with different $\Delta m_{15}(B)$ (e.g. Kasen et al. 2009; M10c). We therefore suggest that the residual could be explained by a combination of the configuration [e.g. the relative contribution between the ECAP/HD and LD zones, which may well be expressed by one parameter i.e. $\Delta m_{15}(B)$] and the viewing angle. Thus, we do not expect a single straight line to give a perfect fit to the residual versus late-time velocity plot. This may be one reason why the correlation in Fig. 8 is not too strong.

8.3 Future perspectives and cosmological applications

Our results could be further tested by polarization measurements. SNe Ia generally show small continuum polarization around the maximum brightness, indicating that they are more or less spherical (e.g. Wang et al. 1996). However, early-phase polarization measurements mainly probe a region near the surface of the SN Ia ejecta, which we also suggest to be nearly spherical. Therefore, the small polarization is likely not a strong argument against our present interpretation. The low continuum polarization is sometimes translated into a small deviation of the photosphere from the spherical symmetry and hence a small dependence of the brightness on the viewing angle (e.g. Höflich et al. 2010). However, this statement depends

[13] Including the effect that the light-curve shape is different for different viewing directions.

strongly on the assumed geometry. For example, a continuum polarization of $\lesssim$0.3 per cent, as is usually found in SNe Ia, implies an axial ratio of less than 10 per cent for an ellipsoidal photosphere (Höflich 1991). However, for a one-sided distribution of ^{56}Ni, as suggested in this work, the expected continuum polarization is generally much smaller than for an ellipsoid (Kasen & Plewa 2007), despite a larger expected variation in the angle-dependent brightness than for the ellipsoidal case (e.g. Sim et al. 2007; Kasen et al. 2009; this work).

There is a correlation between the velocity gradient and the Si II line polarization (Leonard et al. 2005; Chornock & Filippenko 2008; Maund et al. 2010). This may indicate that the viewing direction is indeed controlling the line polarization level, if the velocity gradient is determined by the viewing angle effect (M10b). Further study on the polarization of SNe Ia both in observations (e.g. Wang, Wheeler & Patat 2007) and in theory (e.g. Höflich 1991; Kasen & Plewa 2007) should provide a good test for the geometry of SNe Ia and thus for the results in this work.

A problem in our analysis, especially for the residual issue, is the small sample size. The uncertainty in the distance measurement is also critical in our investigation of the viewing-angle effect on the luminosity residual. We suggest the following strategies to decrease the uncertainty in the distance estimate: (1) obtain late-time spectra for SNe Ia at redshift $z \gtrsim 0.02$. At $z \sim 0.02$, the V-band magnitude of typical SNe Ia at ∼200 d after the maximum brightness is ∼21–22 mag (depending on the extinction). Spectroscopy is thus possible with 6–8 m class telescopes; and (2) obtain comprehensive photometry during both the peak and tail phases. The residual arising from the viewing angle can in principle be seen in the peak-to-tail luminosity ratio, since the effect of the viewing angle vanishes at late phases (e.g. Maeda et al. 2006a). This may provide a distance-independent measurement of the residuals caused by the viewing angle effect. Such observations are less demanding than spectroscopy and thus can reach to larger redshift.

One of the current limitations in the SN Ia cosmology is the fact that a dispersion at the level of ∼0.15 mag remains after the standardization of the peak luminosity with existing relations and that the physical origin of the residual has not been identified. The viewing angle effect may account for part of the dispersion of the SN Ia luminosity calibration, although the presently available sample does not allow us to quantify how much improvement can be achieved by taking this effect into account. However, the effect of the random viewing angle enters in the SN Ia luminosity calibration as a source of a statistic error. Thus, increasing the number of SNe Ia for cosmology should effectively reduce this error in estimating cosmological parameters.

In addition, it may be worthwhile looking into the frequency distribution of the residuals. Although we expect that the statistical error is introduced by random viewing angles, there is no reason to expect it to obey a Gaussian distribution. Investigating a non-Gaussian component in the scatter of the Hubble diagram may provide additional insight. For example, a larger SN Ia sample may allow us to estimate the non-Gaussian contribution to the statistical error, which will then provide a quantitative estimate of the viewing angle effect, independent of uncertainties in the distance measurements for individual SNe.

The result of this work may shed light on how to develop a more accurate SN Ia cosmology than currently employed. The correlation between the colour near the maximum and $v_{\rm neb}$ enables us to discriminate the intrinsic colour and the host extinction when late-time spectra are available. This opens up a possibility of studying the intrinsic colour and the host extinction, including R_V, in detail for nearby SNe up to a redshift of ∼0.02 for which the late-time spectroscopy is possible. This will hopefully provide information about how to distinguish the intrinsic colour and host extinction, the information applicable to high-redshift SNe. The relation between the velocity gradient and the nebular emission-line shift (M10b) suggests that one could use the velocity gradient (accessible to higher redshift SNe) instead of the latter, in the colour and luminosity calibrations (see also Foley & Kasen 2011). Indeed, it has been argued that LVG and HVG SNe should be treated differently in the luminosity calibration (e.g. Wang et al. 2009b). Further investigating relations among these observables (e.g. Fig. 5), as well as finding other observables which correlate with $v_{\rm neb}$, could be useful in improving the colour and luminosity estimates also for high-z SNe Ia.

ACKNOWLEDGMENTS

The authors thank the anonymous referee for many constructive comments. A special thanks to the staff of Gemini South for their efforts in obtaining data and providing user support. This research is supported by the World Premier International Research Center Initiative (WPI Initiative), MEXT, Japan. KM acknowledges financial support by Grant-in-Aid for Scientific Research for Young Scientists (20840007). The work has been partly done during the visit of KM to the MPA supported by the Max-Planck Society and to the Stockholm University supported by the Oskar Klein Centre and the Scandinavia-Japan Sasakawa Foundation. ST acknowledges support by the Transregional Collaborative Research Centre TRR 33 'The Dark Universe' of the German Research Foundation (DFG). MS is supported by the National Science Foundation (NSF) under grant AST–0306969. JS is a Royal Swedish Academy of Sciences Research Fellow supported by a grant from the Knut and Alice Wallenberg Foundation. SB acknowledges partial support from ASI contracts 'COFIS'. MH acknowledges support by FONDECYT Regular 1060808, Centro de Astrofisica FONDAP 15010003, Centro BASAL CATA (PFB 06) and the Millennium Center for Supernova Science (P06-045-F). The Dark Cosmology Centre is funded by the Danish National Research Foundation. This research made use of the SUSPECT (the online Supernova Spectrum Archive) at the Department of Physics and Astronomy, University of Oklahoma, and the HyperLeda data base (http://leda.univ-lyon1.fr).

REFERENCES

Ajhar E. A., Tonry J. L., Blakeslee J. P., Riess A. G., Schmidt B. P., 2001, ApJ, 559, 584
Altavilla G. et al., 2004, MNRAS, 349, 1344
Altavilla G. et al., 2007, A&A, 475, 585
Anupama G. C., Sahu D. K., Jose J., 2005, A&A, 429, 667
Bailey S. et al., 2009, A&A, 500, L17
Benetti S. et al., 2004, MNRAS, 348, 261
Benetti S. et al., 2005, ApJ, 623, 1011
Bongard S., Baron E., Smadja G., Branch D., Hauschildt P. H., 2006, ApJ, 647, 513
Branch D., Drucker W., Jeffery D. J., 1988, ApJ, 330, L117
Branch D. et al., 2003, AJ, 126, 1489
Burns C. R. et al., 2011, AJ, 141, 19
Candia P. et al., 2003, PASP, 115, 277
Cappellaro E., Mazzali P. A., Benetti S., Danziger I. J., Turatto M., della Valle M., Patat F., 1997, A&A, 328, 203
Cappellaro E. et al., 2001, ApJ, 549, L215
Cardelli J. A., Clayton G. C., Mathis J. S., 1989, ApJ, 345, 245

Chornock R., Filippenko A. V., 2008, AJ, 136, 2227
Contardo G., Leibundgut B., Vacca W. D., 2000, A&A, 359, 876
Feldmeier J. J., Jacoby G. H., Phillips M. M., 2007, ApJ, 657, 76
Filippenko A. V. et al., 1992, AJ, 104, 1543
Folatelli G. et al., 2010, AJ, 139, 120 (F10)
Foley R. J., Kasen D., 2011, ApJ, 729, 55
Foley R. J., Filippenko A. V., Jha S. W., 2008, ApJ, 686, 117
Freedman W. L. et al., 2001, ApJ, 553, 47
Gallagher J. S., Garnavich P. M., Berlind P., Challis P., Jha S., Kirshner R. P., 2005, ApJ, 634, 210
Gerardy C. L. et al., 2007, ApJ, 661, 995
Gómez G., López R., Sánchez F., 1996, AJ, 112, 2094
Guy J. et al., 2007, A&A, 466, 11
Hachinger S., Mazzali P. A., Benetti S., 2006, MNRAS, 370, 299
Hachinger S., Mazzali P. A., Tanaka M., Hillebrandt W., Benetti S., 2008, MNRAS, 389, 1087
Hamuy M., Phillips M. M., Wells L. A., Maza J., 1993, PASP, 105, 787
Hamuy M., Phillips M. M., Suntzeff N. B., Schommer R. A., Maza J., Aviles R., 1996, AJ, 112, 2391
Hernandez M. et al., 2000, MNRAS, 319, 223
Hicken M. et al., 2009a, ApJ, 700, 331
Hicken M., Wood-Vasey W. M., Blondin S., Challis P., Jha S., Kelly P. L., Rest A., Kirshner R. P., 2009b, ApJ, 700, 1097
Höflich P., 1991, A&A, 246, 481
Höflich P. et al., 2010, ApJ, 710, 444
Howell A. et al., 2009, ApJ, 691, 661
Iwamoto K., Brachwitz F., Nomoto K., Kishimoto N., Umeda H., Hix W. R., Thielemann F. -K., 1999, ApJS, 125, 439
Jensen J. B., Tonry J. L., Barris B. J., Thompson R. I., Liu M. C., Reike M. J., Ajhar E. A., Blakeslee J. P., 2003, ApJ, 583, 712
Jha S. et al., 1999, ApJS, 125, 73
Jha S., Riess A. G., Kirshner R. P., 2007, ApJ, 659, 122
Kasen D., Plewa T., 2007, ApJ, 662, 459
Kasen D., Röpke F. K., Woosley S. E., 2009, Nat, 460, 869
Kelly P. L., Hicken M., Burke D. L., Mandel K. S., Kirshner R. P., 2010, ApJ, 715, 743
Kelson D. D. et al., 2000, ApJ, 529, 768
Kessler R. et al., 2009, ApJ, 185, 32
Khokhlov A., 1991, A&A, 245, 114
Kotak R. et al., 2005, A&A, 436, 1021
Krisciunas K., Hastings N. C., Loomis K., McMillan R., Rest A., Riess A. G., Stubbs C., 2000, ApJ, 539, 658
Krisciunas K. et al., 2001, AJ, 122, 1616
Krisciunas K. et al., 2003, AJ, 125, 166
Krisciunas K. et al., 2004, AJ, 128, 3034
Krisciunas K. et al., 2007, AJ, 133, 58
Krisciunas K. et al., 2009, AJ, 138, 1584
Kuhlen M., Woosley S. E., Glatzmaier G. A., 2006, ApJ, 640, 407
Lampeitl H. et al., 2010, ApJ, 722, 566
Leibundgut B., 2008, Gen. Relativ. Gravit., 40, 221
Leloudas G. et al., 2009, A&A, 505, 265
Leonard D. C., 2007, In: Immler S., Weiler K., eds, AIP Conf. Proc. Vol. 937, Constraining the Type Ia Supernova Progenitor: The Search for Hydrogen in Nebular Spectra. Am. Inst. Phys., New York, p. 311
Leonard D. C., Li W., Filippenko A. V., Foley R. J., Choronock R., 2005, ApJ, 632, 450
Li W. et al., 2001, PASP, 113, 1178
Lira P. et al., 1998, AJ, 116, 1006
Lucy L. B., 2005, A&A, 429, 19
Maeda K., 2006, ApJ, 644, 385
Maeda K., Mazzali P. A., Nomoto K., 2006a, ApJ, 645, 1331
Maeda K., Nomoto K., Mazzali P. A., Deng J., 2006b, ApJ, 640, 854
Maeda K., Taubenberger S., Sollerman J., Mazzali P. A., Leloudas G., Nomoto K., Motohara K., 2010a, ApJ, 708, 1703 (M10a)
Maeda K. et al., 2010b, Nat, 466, 82 (M10b)
Maeda K., Röpke F. K., Fink M., Hillebrandt W., Travaglio C., Thielemann F.-K., 2010c, ApJ, 712, 624 (M10c)
Mattila S., Lundqvist P., Sollerman J., Kozma C., Baron E., Fransson C., Leibundgut B., Nomoto K., 2005, A&A, 443, 649
Maund J. R. et al., 2010, ApJ, 725, L167
Mazzali P. A., Podsiadlowski Ph., 2006, MNRAS, 369, L19
Mazzali P. A., Cappellaro E., Danziger I. J., Turatto M., Benetti S., 1998, ApJ, 499, L49
Mazzali P. A., Nomoto K., Cappellaro E., Nakamura T., Umeda H., Iwamoto K., 2001, ApJ, 547, 988
Mazzali P. A., Röpke F. K., Benetti S., Hillebrandt W., 2007, Sci, 315, 825
Morrell N., Folatelli G., Stritzinger M., 2007, Cent. Bur. Electron. Telegrams, 1131, 1
Motohara K. et al., 2006, ApJ, 652, L101
Neill J. D. et al., 2009, ApJ, 707, 1449
Nugent P., Phillips M., Baron E., Branch D., Hauschildt P., 1995, ApJ, 455, L147
Nugent P., Kim A., Perlmutter S., 2002, PASP, 114, 803
Pastorello A. et al., 2007a, MNRAS, 377, 1531
Pastorello A. et al., 2007b, MNRAS, 376, 1301
Patat F., Benetti S., Cappellaro E., Danziger I. J., Della Valle M., Mazzali P. A., Turatto M., 1996, MNRAS, 278, 111
Paturel G., Garcia A. M., Fouque P., Buta R., 1991, A&A, 243, 319
Paturel G., Petit C., Prugniel Ph., Theureau G., Rousseau J., Brouty M., Dubois P., Cambrésy L., 2003, A&A, 412, 45
Phillips M. M., 1993, ApJ, 413, L105
Phillips M. M., Lira P., Suntzeff N. B., Schommer R. A., Hamuy M., Jose M., 1999, AJ, 118, 1766
Pignata G. et al., 2004, MNRAS, 355, 178
Pignata G. et al., 2008, MNRAS, 388, 971
Prieto J. L., Rest A., Suntzeff N. B., 2006, ApJ, 647, 501
Reindl B., Tammann G. A., Sandage A., Saha A., 2005, ApJ, 624, 532
Richmond M. W. et al., 1995, AJ, 109, 2121
Rieke G. H., Lebofsky M. J., 1985, ApJ, 288, 618
Riess A. G. et al., 1999, AJ, 118, 2675
Riess A. G. et al., 2005, ApJ, 627, 579
Riess A. G. et al., 2009, ApJ, 699, 539
Röpke F. K., Niemeyer J. C., 2007, A&A, 464, 683
Saha A., Thim F., Tammann G. A., Reindl B., Sandage A., 2006, ApJS, 165, 108
Saviane I., Momany Y., da Costa G. S., Rich R. M., Hibbard J. E., 2008, ApJ, 678, 179
Schlegel D. J., Finkbeiner D. P., Davis M., 1998, ApJ, 500, 525
Schweizer F. et al., 2008, AJ, 136, 1482
Seitenzahl I. R., Röpke F. K., Fink M., Pakmor R., 2010, MNRAS, 407, 2297
Sim S. A., Sauer D. N., Röpke F. K., Hillebrandt W., 2007, MNRAS, 378, 2
Sollerman J. et al., 2004, A&A, 428, 555
Stanishev V. et al., 2007, A&A, 469, 645
Stehle M., Mazzali P. A., Benetti S., Hillebrandt W., 2005, MNRAS, 360, 1231
Stetson P. B., Gibson B. K., 2001, MNRAS, 328, L1
Stritzinger M., Leibundgut B., 2005, A&A, 431, 423
Stritzinger M., Leidbundgut B., Walch S., Contardo G., 2006, A&A, 450, 241
Stritzinger M. et al., 2010, AJ, 140, 2036
Sullivan M. et al., 2010, MNRAS, 406, 782
Tanaka M., Mazzali P. A., Maeda K., Nomoto K., 2006, ApJ, 645, 470
Tanaka M., Maeda K., Mazzali P. A., Nomoto K., 2007, ApJ, 668, L19
Tanaka M. et al., 2008, ApJ, 677, 448
Timmes F. X., Brown E. F., Truran J. W., 2003, ApJ, 590, L83
Tonry J. L., Dressler A., Blakeslee J. P. Ajhar E. A., Fletcher A. B., Luppino G. A., Metzger M. R., Moore C. B., 2001, ApJ, 546, 681
Tripp R., 1998, A&A, 331, 815
Tripp R., Branch D., 1999, ApJ, 525, 209
Turatto M., Benetti S., Cappellaro E., Danziger I. J., Della Valle M., Gouiffes C., Mazzali P. A., Patat F., 1996, MNRAS, 283, 1
Wang L., Wheeler J. C., Li Z., Clocchiatti A., 1996, ApJ, 467, 435
Wang L., Wheeler J. C., Patat F., 2007, Sci, 315, 212

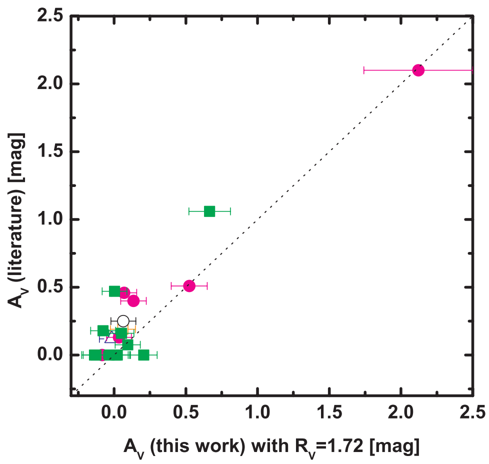

Figure A1. Comparison of the extinction. The horizontal axis denotes the values of A_V derived in this study (Table 2), while the vertical axis provides values from the literature (Table A1). The symbols and colour-coding indicate the velocity gradient near the maximum brightness (see Fig. 4).

Wang X., Wang L., Pein R., Zhou Xu, Li Z., 2006, ApJ, 645, 488
Wang X. et al., 2008, ApJ, 675, 626
Wang X. et al., 2009a, ApJ, 697, 380
Wang X. et al., 2009b, ApJ, 699, L139
Willick J. A., Courteau S., Faber S. M., Burstein D., Dekel A., Strauss M. A., 1997, ApJS, 109, 333
Wood-Vasey W. M. et al., 2007, ApJ, 666, 694
Woosley S. E., Weaver T. A., 1994, ApJ, 423, 371
Yamanaka M. et al., 2009, PASJ, 61, 713
Yamaoka H., Shigeyama T., Nomoto K., Thielemann F.-K., 1992, ApJ, 393, L55
Yasuda N., Fukugita M., 2010, AJ, 139, 39
Yu B., Yang G., Lu T., 2009, preprint (arXiv:0910.5638)

APPENDIX A: EXTINCTIONS AS COMPARED TO OTHER ESTIMATES

In Section 4, we compared the colour excesses we derived (with $v_{\rm neb}$) to those estimated by Wang et al. (2009b). As a further, additional test, we also check how our extinction values compare to those previously estimated and presented in the literature by different methods. Assuming $R_V = 1.72$ (Sections 1 and 5), we convert $E(B-V)$ to A_V. Fig. A1 shows a comparison between A_V as derived in this study and the values from the literature. The literature values were selected as follows: if optical minus NIR (i.e. $V-K$, $V-J$, $V-H$) colour curves are available, the template colour curves of Krisciunas et al. (2000, 2001, 2009) were used to derive A_V with the IR extinction law given by Rieke & Lebofsky (1985). A similar estimate is also possible using the NIR spectral energy distribution at a single epoch [e.g. Wang et al. (2008), who used the extinction law of Cardelli, Clayton & Mathis (1989) constructed from the data provided by Rieke & Lebofsky (1985)]. For SN 2001el, the value of A_V was taken from Krisciunas et al. (2007) who used SN 2004S as a template because of the similarity between these two events. When these NIR measurements were available, we adopted A_V based on these estimates. When NIR measurements were not available, we converted $E(B-V)$ colour excess estimates *from the literature* to A_V using $R_V = 1.72$. In the cases of SNe 2007sr (Schweizer et al. 2008), 2007on and 2009ab (Stritzinger et al., in preparation), $E(B-V)$ was obtained using the template light-curve fitter SNooPy (Burns et al. 2011). The values thus compiled are listed in Table A1.

Table A1. Extinction from the literature.

SN	A_V (mag)	Method	Reference[a]
1990N	0.16		Ph99
1994D	0.0		Ph99
1997bp	0.46		A04
1998aq	0.0		W09b
1998bu	1.06	NIR	K00
2000cx	0.0		L01
2001el	0.47	NIR	K07
2002bo	0.51	NIR	K04
2002dj	0.0	NIR	P08
2002er	0.40		W09b
2003du	0.0	NIR	S07
2003hv	0.0		L09
2004dt	0.19		W09b
2004eo	0.0	NIR	P07
2005cf	0.18	NIR	W09a
2006X	2.1	NIR	W08
2006dd	0.12		S10a
2007on	0.25		S10b
2007sr	0.13		S10b
2009ab	0.076		S10b

[a]*References*: A04: Altavilla et al. (2004); K00: Krisciunas et al. (2000); K04: Krisciunas et al. (2004); K07: Krisciunas et al. (2007); L01: Li et al. (2001); L09: Leloudas et al. (2009); P07: Pastorello et al. (2007a); P08: Pignata et al. (2008); Ph99: Phillips et al. (1999); S07: Stanishev et al. (2007); S10a: Stritzinger et al. (2010); S10b: Stritzinger et al. (in prep.); W08: Wang et al. (2008); W09a: Wang et al. (2009a); and W09b: Wang et al. (2009b).

From this comparison, we find the similar results to those obtained by the comparison to $E(B-V)$ derived by Wang et al. (2009b). Our estimates tend to be smaller, and even if we assume $R_V \sim 3$ to convert our $E(B-V)$ estimate to A_V, the extinctions we derive are mostly consistent with those derived by the other method (except for the heavily reddened SN 2006X).

APPENDIX B: UNCERTAINTIES IN THE LUMINOSITY CALIBRATION

Compared to the colour calibration (Section 4), our analysis on the luminosity residual (Section 6) suffers from various sources of uncertainties. These are independent of $v_{\rm neb}$ and so it is unlikely that any correlation we investigate in this study is artificially introduced by these uncertainties in a systematic way. However, our present sample is still small and thus statistical errors due to these uncertainties can still be important. In this section, we investigate how our results in Section 6 are affected by changing the procedures to estimate the distance, reddening and standardized luminosity (Section 5). Results are summarized in Table B1. Each item in the table is explained in the following.

B1 Distances

To examine the uncertainty in the distances, we first compare the distances obtained by different methods, when available, in Fig. B1. HF distances with a recession velocity below 1000 km s^{-1} are not considered as alternatives here. Different measurements typically agree with each other to within the errors (albeit these errors are sometimes quite large, when only the HF distances are available as

Table B1. Relations between $v_{\rm neb}$ and dm.

Description	N^a	α^b	β	P^c	Significance
Distance[d]	20	$0.092 \pm 0..052$	0.070 ± 0.077	0.038	1.8σ
STS[e]	20	0.11 ± 0.050	-0.013 ± 0.076	0.016	2.1σ
R_V[f]	20	0.072 ± 0.055	0.040 ± 0.082	0.099	1.3σ
A_V (literature)[g]	20	0.050 ± 0.049	-0.064 ± 0.074	0.16	1.0σ
$\bar{M}_V(\Delta m_{15}(B))$[h]	20	0.081 ± 0.051	0.071 ± 0.077	0.059	1.6σ

[a]The number of SNe.
[b]The best fit using the relation d$m = \alpha\,(v_{\rm neb}/1000\,{\rm km\,s^{-1}}) + \beta$ mag. The errors for α and β are 1σ uncertainties.
[c]Probability that the distribution arises from a non-correlation.
[d]Obtained by changing the distances to SNe 1990N and 2006dd (Section B1).
[e]Obtained by changing the distances to the STS scale (Section B1, Table B2).
[f]With $R_V = 3.1$ (Section B2).
[g]A_V adopted from the literature (Section B2).
[h]The reference magnitude changed to that of Phillips et al. (1999) (Section B3).

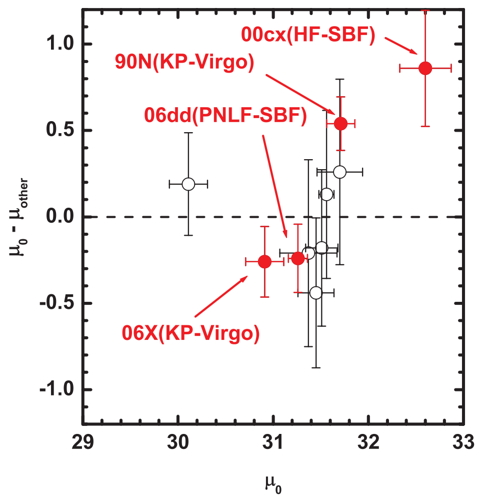

Figure B1. Comparison of the distance we adopted (μ_0) and that from a different method ($\mu_{\rm other}$) for SNe with several independent distance measurements available. The SNe discussed in Section B1 are marked with the red-filled circles and indicated by SN ($\mu_0 - \mu_{\rm other}$).

the ‘other’ measurement). However, there are several exceptions. NGC 4639 (SN 1990N) and NGC 4321 (SN 2006X) are (possible) members of the Virgo cluster. If we adopt the distance modulus $\mu = 31.17 \pm 0.04$ mag for the Virgo cluster (Kelson et al. 2000), it differs significantly from the Cepheid distance to NGC 4639 we adopted [μ(KP) $= 31.71 \pm 0.15$ mag]. We note, however, that Riess et al. (2009) revised the Cepheid distance to NGC 4639 to be $\sim$31.48 $\pm$ 0.13 mag. Although there is still a discrepancy between the distances to NGC 4639 and the Virgo cluster, this new measurement makes the agreement better. If we adopt the value of Riess et al. (2009), SN 1990N should be fainter by 0.23 mag than our fiducial estimate. We did not adopt this value in the main text to avoid possible systematic errors in different Cepheid measurements. The distance to NGC 524, the host of SN 2000cx, is 31.74 ± 0.20 mag (SBF) or 32.60 ± 0.27 mag (HF), which clearly do not agree with each other. Although we usually adopt the SBF distance as the better estimate, we note that another supernova, SN 2008Q, appeared in the same galaxy and *both* of these SNe would be peculiar outliers in this case. Thus, we adopted the HF distance to SN 2000cx (Section 3). Finally, the PNLF distance ($\mu = 31.26 \pm 0.1$ mag) to NGC 1316 (SN 2006dd) is smaller than the SBF distance ($\mu = 31.50 \pm 0.17$)

Table B2. SN Ia sample on the STS distance scale.

SN	Host	μ (mag)
1990N	NGC 4639	32.20 ± 0.09 (STS)
1994D	NGC 4526	31.18 ± 0.20 (SBF)
1998aq	NGC 3982	31.87 ± 0.15 (STS)
1998bu	NGC 3368	30.34 ± 0.11 (STS)
2002bo	NGC 3190	31.90 ± 0.24 (SBF)
2003hv	NGC 1201	31.57 ± 0.3 (SBF)
2006X	NGC 4321	31.18 ± 0.05 (STS)
2007on	NGC 1404	31.65 ± 0.19 (SBF)

and Stritzinger et al. (2010) argued that the former is more accurate (thus adopted in the main text).

Following the above inspection, we change the distance to SN 1990N (from the original KP value to that derived by Riess et al. 2009) and that to SN 2006dd (from the PNLF to the SBF), and repeat the same analysis as we did in Fig. 8. We thereby obtain a chance probability of $P = 0.038$ (1.8σ) (Table B1).

As another test, we explore how our results are affected if we adopt the STS Cepheid distances (Section 5). For four SNe Ia with a Cepheid distance available, there are also measurements by the STS group (Saha et al. 2006). We also change the SBF measurements to be consistent with the STS measurements. The SBF values used in the main text are calibrated with the KP Cepheid distance zero-point. Since the STS values are on average larger than the KP values by $\sim$0.2 mag, we add 0.2 mag for the SBF distances. Table B2 lists the STS distances thus derived for SNe Ia. For SNe Ia missing in Table B2, the same distances as in Table 1 are used. Fig. B2 shows the $v_{\rm neb}$ versus dm diagram with the STS distance scale. For 20 SNe Ia, we obtained a chance probability of $P = 0.016$ (2.1σ). The slope of the linear fit is steeper than that derived with the KP distance scale, although they are consistent within the errors of the fits. The zero-point is displaced by $\sim$0.1 mag, reflecting the difference between the STS and KP distance scales.

B2 Extinction

Another large uncertainty comes from the estimate of the extinction within the host galaxies. To check the uncertainty, we change the value of R_V to 3.1, the standard value for Galactic extinction.

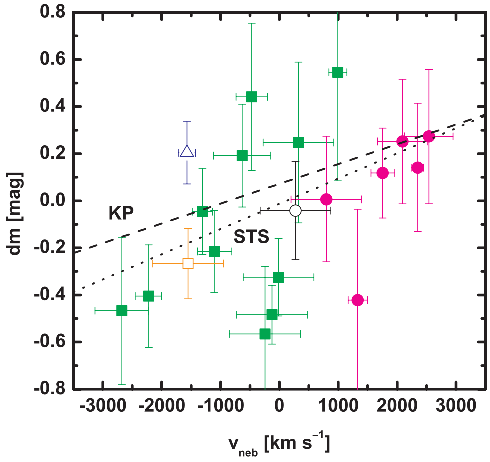

Figure B2. The same as Fig. 8, but using the STS measurements for the Cepheid distances and a revised zero-point for the SBF distances. See the caption of Fig. 4 for the meaning of the different symbols. The dotted line is the best-fitting line for the STS distances, while the dashed line is that for the KP distances.

Following Section 4 and F10, R_V for SN 2006X is left unchanged. While it has been argued that the typical Galactic value is not necessarily applicable for the host galaxies of SNe Ia (e.g. Hicken et al. 2009a,b; Wang et al. 2009b; Folatelli et al. 2010; Yasuda & Fukugita 2010), our analysis in Section 4 suggests that an R_V close to the typical Galactic value can be acceptable for mildly extinguished SNe, once the intrinsic colour variation due to the viewing direction is taken into account. Figure B3 shows the $v_{\rm neb}$–dm diagram with $R_V = 3.1$. We obtain linear fit parameters as follows: $P = 0.099$ (1.3σ). The best-fitting lines for different R_V (1.72 and 3.1) are consistent to each other within the fitting errors. The significance of the fit is slightly weaker for $R_V = 3.1$ than in our fiducial case. It is, however, a reasonably large range of R_V that we investigate.

Next, we explore whether our use of the relation between $v_{\rm neb}$ and the colour to derive the extinction might affect the results. For this purpose, we replace the host galaxy extinction by the values given in the literature and repeat the same analysis. For the literature values, see Table A1 and the related discussion in the main text. The result is shown in Fig. B4. The fitting result is $P = 0.16$ (1.0σ) (Table B1). Although there is still a correlation, it is weaker than if the $v_{\rm neb}$–colour relation derived in this paper is adopted (1.6σ).

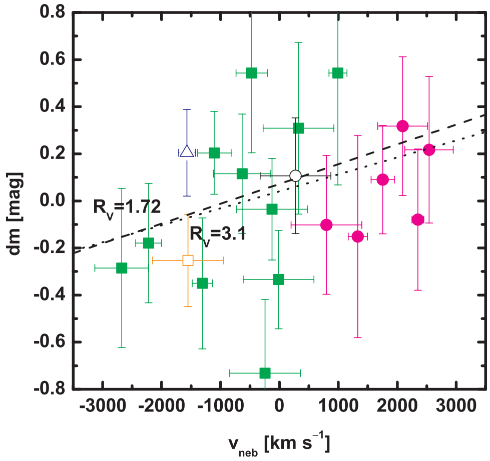

Figure B3. The same as Fig. 8, but using $R_V = 3.1$ for the extinction. See the caption of Fig. 4 for the meaning of the different symbols. The dotted line is the best-fitting line for the data points with $R_V = 3.1$, while the dashed line is for the fiducial value of $R_V = 1.72$.

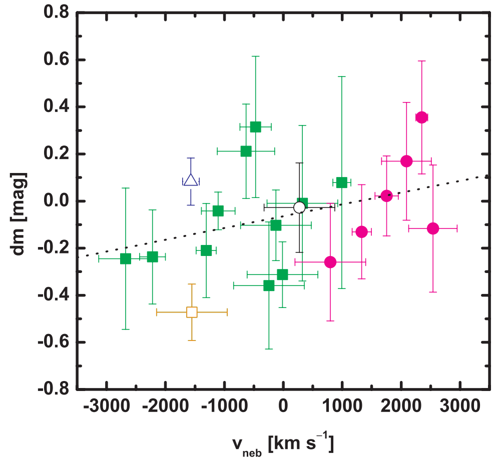

Figure B4. The same as Fig. 8, but A_V replaced by the values in the literature (Table A1). The best-fitting line is shown by the dotted line.

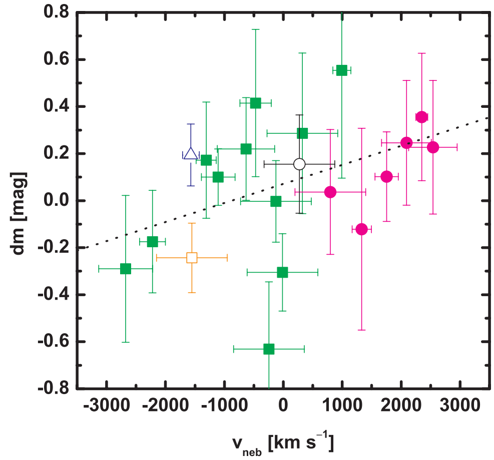

Figure B5. The same as Fig. 8, but using the original Phillips relation (Phillips et al. 1999) for the reference magnitude [$\bar{M}_V(\Delta m_{15}(B))$]. See the caption of Fig. 4 for the meaning of the different symbols. The dotted line is the best-fitting line for this data set.

B3 Standardized luminosities

By definition, dm depends on the standardized luminosity, that is, $\bar{M}_V(\Delta m_{15}(B))$. We have used an updated relation given by F10. To check the related uncertainty, we replace $\bar{M}_V(\Delta m_{15}(B))$ by the original version of the Phillips relation, including the second-order term in $\Delta m_{15}(B)$ (Phillips et al. 1999) and repeat the same analysis. $\bar{M}_V(\Delta m_{15}(B) = 1.1)$ is set to be -19.12 mag, to be consistent with Folatelli et al. (2010). Fig. B5 shows the resulting $v_{\rm neb}$–dm diagram. We obtain $P = 0.059$ (1.6σ).

APPENDIX C: MONTE CARLO SIMULATION FOR ESTIMATING THE CHANCE PROBABILITY

To estimate the chance probability P that a distribution arises from a non-correlation in Section 6, we have used the following method based on Monte Carlo simulations: we performed a linear regression to a set of variables ($X_i \pm \sigma_{X_i}$, $Y_i \pm \sigma_{Y_i}$) (where i spans the numbers in the SN sample). First, we produced 10^5 test distributions obtaining ($X'_{i,k}$, $Y'_{i,k}$) (with k spanning from 1 to 10^5), where a Gaussian distribution is assumed for the variation in X_i and Y_i with the associated errors σ_{X_i} and σ_{Y_i}. Here, σ_{Y_i} includes both the extinction and the distance uncertainties. For each kth test distribution, we performed a linear regression fitting assuming the functional form $Y' = \alpha_k X' + \beta_k$. Here we used only the error associated with the extinction as a weight in the χ^2 fitting for each distribution, because the 'relative' errors between different distance measurements are difficult to quantify. We thereby obtained $\alpha_k = \alpha_{k,0} \pm \sigma_{\alpha_k}$ and $\beta_k = \beta_{k,0} \pm \sigma_{\beta_k}$ by the linear regression for each kth test distribution. This results in a probability distribution of the fitting coefficients, α and β, by convolving 10^5 Gaussian distributions for α_k and β_k. The final fitting result is then obtained by fitting Gaussian profiles to the probability distribution of α and β. To estimate the chance probability P that the distribution ($X \pm \sigma_X$, $Y \pm \sigma_Y$) would arise from a non-correlation, we counted the probability for $\alpha \leq 0$ (if the mean value of α is positive).

This paper has been typeset from a TEX/LATEX file prepared by the author.